Free Radical Biology and Medicine 112 (2017) 174–190

Contents lists available at ScienceDirect

Free Radical Biology and Medicine

journal homepage: www.elsevier.com/locate/freeradbiomed

Activation of brain glucose metabolism ameliorating cognitive impairment in APP/PS1 transgenic mice by electroacupuncture

Weilin Liu[a,1], Peiyuan Zhuo[b,1], Long Li[b], Hao Jin[b], Bingbing Lin[b], Yingzheng Zhang[b], Shengxiang Liang[c], Jie Wu[b], Jia Huang[a], Zhifu Wang[b], Ruhui Lin[b], Lidian Chen[a,*], Jing Tao[a,*]

[a] College of Rehabilitation Medicine, Fujian University of Traditional Chinese Medicine, Fuzhou, Fujian 350122, China
[b] Fujian Key Laboratory of Rehabilitation Technology, Fuzhou, Fujian 350122, China
[c] Division of Nuclear Technology and Applications, Institute of High Energy Physics, Chinese Academy of Sciences, Beijing 100049, China

ARTICLE INFO

Keywords:
Electroacupuncture
Alzheimer's disease
Glucose metabolism
Cognitive impairment
^{18}F-Fluoro-2-deoxy-D-Glucose
Adenosine monophosphate-activated protein kinase
AKT

ABSTRACT

An essential feature of Alzheimer's disease (AD) is implicated in brain energy metabolic impairment that is considered underlying pathogenesis of cognitive impairment. Therefore, therapeutic interventions to allay cognitive deficits that target energy metabolism may be an efficacy strategy in AD. In this study, we found that electroacupuncture (EA) at the DU20 acupoint obviously increased glucose metabolism in specific brain regions such as cortex, hippocampus, cingulate gyrus, basal forebrain septum, brain stem, and cerebellum in APP/PS1 transgenic mice by animal ^{18}F-Fluoro-2-deoxy-D-Glucose (^{18}F-FDG)/positron emission tomography (PET) imaging, accompanied by cognitive improvements in the spatial reference learning and memory and memory flexibility and novel object recognition performances. Further evidence shown energy metabolism occurred in neurons or non-neuronal cells of the cortex and hippocampus in terms of the co-location of GLUT3/NeuN and GLUT1/GFAP. Simultaneously, metabolic homeostatic factors were critical for glucose metabolism, including phosphorylated adenosine monophosphate-activated protein kinase (AMPK) and AKT serine/threonine kinase. Furthermore, EA-induced phosphorylated AMPK and AKT inhibited the phosphorylation level of the mammalian target of rapamycin (mTOR) to decrease the accumulation of amyloid-beta (Aβ) in the cortex and hippocampus. These findings are concluded that EA is a potential therapeutic target for delaying memory decline and Aβ deposition of AD. The AMPK and AKT are implicated in the EA-induced cortical and hippocampal energy metabolism, which served as a contributor to improving cognitive function and Aβ deposition in a transgenic mouse model of AD.

1. Introduction

Alzheimer's disease (AD) is an age-related neurodegenerative disorder with progressive memory deficits and cognitive impairments [1]. It is estimated to have more than 30 million AD patients worldwide in 2010 and an expected 106 million by 2050 [2]. However, there is not an absolutely effective treatment which can prevent the onset and progression of cognitive impairment in AD [3]. Thus, the identification of effective and safe treatments with clear functional mechanisms is urgently needed.

Ample clinical evidence has showed that electroacupuncture (EA), penetrated specific acupoints of the skin with needles and engrafted electric stimulation, is a potential therapy for improving learning and memory ability of AD [4,5]. Stimulation of Baihui (DU 20) acupoint, located at the intersection of the sagittal midline and the line linking two rat ears, generates a specific pathway (meridian, and qi) to nourish the brain described in traditional Chinese medicine (TCM). Our previous studies have demonstrated that EA at the DU 20 acupoint could improve cognitive deficits in animal models of AD [6], and the other teams also provide support [7]. However, the functional mechanisms of EA treatment for delaying memory loss of AD is far from been fully elucidated.

AD is characterized by accumulations of amyloid-beta (Aβ) peptide known as plaques and neurofibrillary tangles and neuronal loss in

Abbreviations: AD, Alzheimer's disease; EA, electroacupuncture; ^{18}F-FDG, ^{18}F-Fluoro-2-deoxy-D-Glucose; PET, positron emission tomography; AMPK, adenosine monophosphate-activated protein kinase; mTOR, mammalian target of rapamycin; Aβ, amyloid-beta; ThS, Thioflavin staining; MWM, Morris water maze; NOR, novel object recognition; ELISA, Enzyme-linked immunosorbent assay; IHC, Immunohistochemistry

* Corresponding authors.
E-mail addresses: cld@fjtcm.edu.cn (L. Chen), taojing01@163.com (J. Tao).
[1] These authors contributed equally to this work.

http://dx.doi.org/10.1016/j.freeradbiomed.2017.07.024
Received 22 October 2016; Received in revised form 24 July 2017; Accepted 25 July 2017
Available online 26 July 2017

several areas of the brain [8]. Moreover, an essential feature of AD is implicated in brain energy metabolic impairments [9–11]. A reduction of glucose metabolism as seen on PET in the posterior cingulate and in the temporal-parietal regions is the most commonly described diagnostic criterion for AD [12,13]. Studies have suggested that the cognitive decline of AD to a certain extent results from the low level of glucose uptake in brain regions that include hippocampus, amygdala, posterior cingulate cortex, and right lateral parietal region [14,15]. A number of transgenic mouse models of AD show abnormalities in glucose metabolism in brain regions with homology to those affected in clinical AD, including hippocampus, and cortex, in which regional metabolic changes are associated with learning and memory impairment in those models of AD [16–18]. Additionally, Aβ oligomer formation generate reactive oxygen species that cause in impairment function of membrane ion-motive (Ca^{2+} and Na^{+}/K^{+}) ATPases and glucose transporter proteins, which, conversely, a prolonged positive energy metabolic stress impairs the ability of neurons to respond adaptively to oxidative and Aβ metabolism and cognitive impairment [19,20].

Furthermore, well-documented findings display that the functional abnormities of critical metabolic sensors, including adenosine monophosphate-activated protein kinase (AMPK) and AKT serine/threonine kinase, cause energy metabolic impairment, which has been proved to implicate in AD pathology [21,22]. The Aβ oligomers can transiently inhibit AMPK and AKT phosphorylation levels and cause neuronal metabolic defects [23,24]. Therefore, therapeutic interventions to allay cognitive deficits and Aβ-induced neurological damage that target AMPK or AKT have shown efficacy in animal models and preliminary studies in humans [25,26]. Interestingly, several studies have demonstrated that EA can activate AMPK and AKT expression in rodents' models of AD [27,28]. Therefore, we speculated that EA could increase energy metabolism for effectively delaying cognitive decline in AD. In addition, ^{18}F-FDG/PET imaging is a scanning technique in vivo and becomes available for visualizing cerebral metabolic glucose metabolic processes in small rodents [29]. Based on these findings, the current study aimed to reveal whether EA treatment could alleviate cognitive impairment via increasing brain regional AMPK and AKT-mediated glucose metabolism, assessed by longitudinal monitoring of small animal ^{18}F-FDG/PET imaging before and after treatment in AD transgenic model mice.

2. Materials and methods

2.1. Materials and reagents

3,3′-diaminobenzidine (DAB) kits (Kit-0017) were purchased from Fuzhou Maixin Biotech, Co., Ltd. (Fuzhou, China). Polyclonal rabbit anti-Aβ (1-42) (cat. no.ab10148), GLUT1 (cat. no.ab652) GFAP (cat.-no.ab49874), MAP2 (cat.no.ab36447) and NeuN (cat.no.ab104224) antibody were obtained from Abcam (Cambridge, UK). Polyclonal rabbit GLUT3 (cat. no.bs-1207R) was obtained from BIOSS (Beijing, China). AKT antibody (cat. no.4691S), phospho-AKT antibody (Ser473, cat. no.4060S), mTOR antibody (cat. no.2972), phospho-mTOR antibody (Ser2448, no. 5536), AMPK antibody (cat. no.2532S) and phospho-AMPK (Thr172) antibody (cat. no.2531S), were obtained from Cell Signaling Technology, Inc. (Danvers, MA, USA). The horseradish peroxidase (HRP)-conjugated monoclonal goat secondary antibodies [anti-rat IgG (cat. no. 7077S) and anti-rabbit IgG (cat. no. 7074P2)] were also obtained from Cell Signaling Technology, Inc. All other chemicals used, unless otherwise stated, were obtained from Beyotime Institute of Biotechnology (Haimen, China).

2.2. Animals and ethics

Nine-month-old female APP/PS1 double-transgenic mice [B6C3-Tg (APPswe, PSEN1dE9) 85Dbo/MmJNju], and age-matched wild-type littermates were obtained from Nanjing Biomedical Research Institute of Nanjing University (Nanjing, China, no.201402397). Each mouse was housed in a plastic cage in a controlled environment (22–25 °C; 50 ± 10% relative humidity and automatic 12-h light/dark cycle) with access to food and water ad libitum. All animals were maintained in a specific pathogen-free environment for two months prior to being sacrificed. Furthermore, the experiments were approved by the Committee of Fujian University of Traditional Chinese Medicine, and were strictly in accordance with international ethical guidelines and the National Institutes of Health Guide for the Care and Use of Laboratory Animals.

2.3. Experimental protocol

Mice were randomly divided into four groups according to the random number table (n = 10 each group): i) wild-type group (WT); ii) APP/PS1group (APP/PS1); iii) APP/PS1 mice with repeated EA at the DU 20 acupoint administration (APP/PS1 + EA); and iiii) APP/PS1 mice with repeated EA at the non-acupoint administration (APP/PS1 + Non-EA). The mice in APP/PS1 + EA group was administered EA for 30 min, 5 days/week, and 2 days rest for a period of 4 weeks. The EA needles (diameter, 0.3 mm, Huatuo acupuncture of Suzhou Co., Ltd., Suzhou China) were inserted at a depth of 2–3 mm into the DU20 acupoint, which is located at the intersection of the sagittal midline and the line linking the two ears. Stimulation was generated using EA apparatus (model G6805; Suzhou Medical Appliance Factory, Shanghai, China) and the stimulation parameters were set as disperse waves of 1 and 20 Hz. In the APP/PS1 + Non-EA group, a non-acupoint (the area below the costal region, 2 cm superior to the posterior superior iliac spine and ~ 3 cm lateral to the spine) was punctured and stimulated for 30 min, 5 days/week, and 2 days rest for a period of 4 weeks [30]. The APP/PS1 + EA and the APP/PS1 + Non-EA groups received treatment with the same needles, stimulation parameters and EA apparatus. The experimental timeline is shown in Fig. 1.

2.4. Morris water maze test

Before and after 4 weeks of EA treatment, cognitive function was tested by the Morris water maze apparatus (Chinese Academy of Sciences, Beijing, China), which was a stainless steel circular tank with a diameter of 120 cm and a height of 50 cm. The tank was filled with water (21–23 °C) to the depth of 40 cm and divided into four equal quadrants. A platform (diameter, 6 cm) was placed in the third quadrant and submerged 1 cm below the surface of the water. For the place navigation trials, mice were trained for four days. Each trial was started by placing the mice in one of the four quadrants. Mice were allowed to swim in pool during a period of 90 s to find the hidden platform. If a mouse did not find the platform within 90 s, it would be removed from the water and placed on the platform for 15 s by researchers. On the fifth day, the probe trail test was performed to assess spatial reference

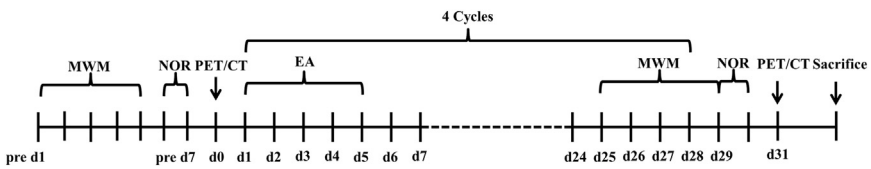

Fig. 1. Schematic representation of the methodology used. Morris water maze (MWM) and novel object recognition (NOR) and PET/CT test was performed before and after EA treatment in nine-month APP/PS1 mice. EA treatment was administered for 30 min/day, 5 days per week, and 2 days rest for 4 weeks. Mice used for other studies were sacrificed after the PET/CT scan.

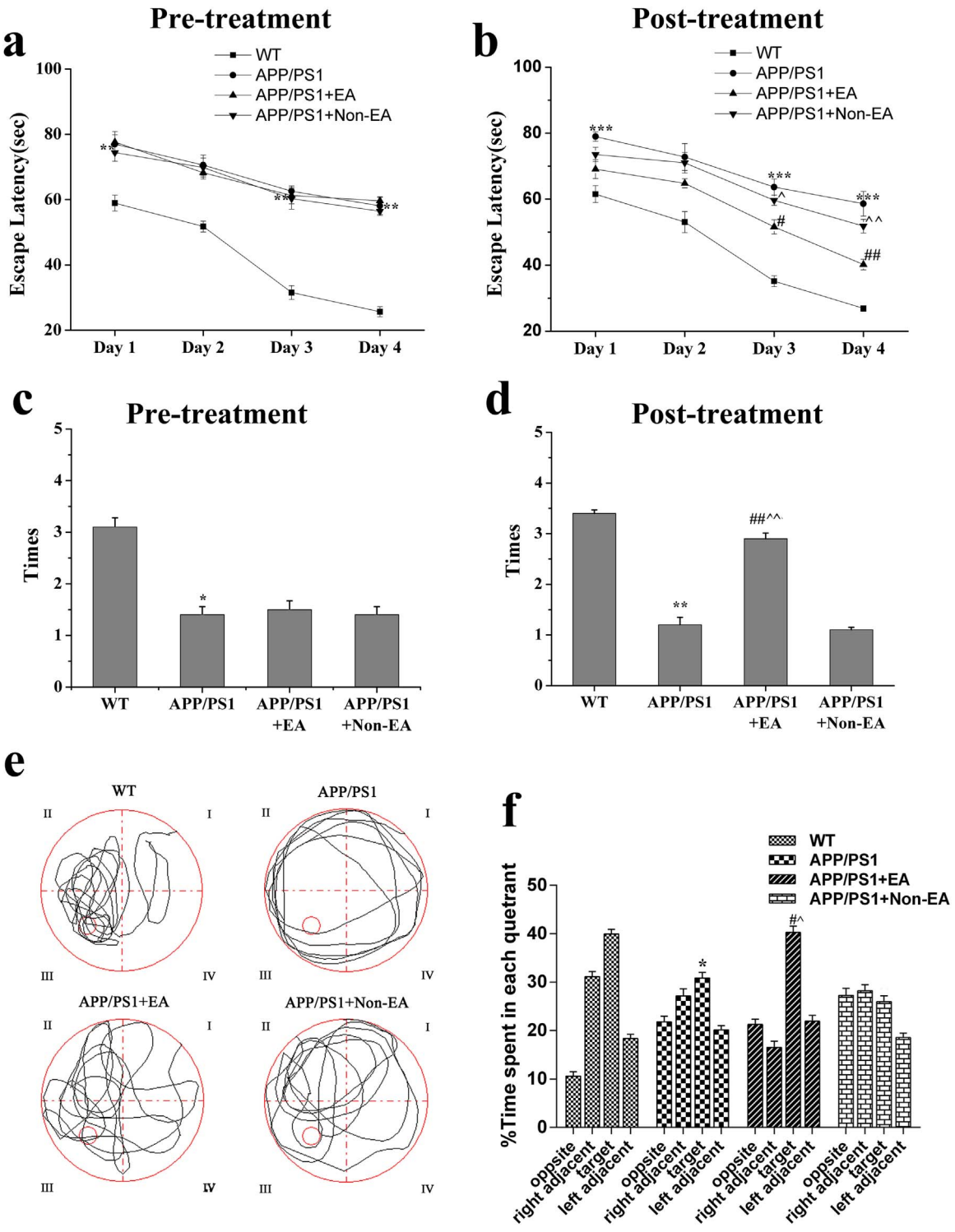

Fig. 2. EA delayed learning and memory decline in the APP/PS1 mice. (a and b) The escape latency during the orientation navigation in MWM test at pre-treatment and post-treatment. (c and d) The times of passing the hidden platform position at pre-treatment and post-treatment. (e) Representative navigation traces of different swimming strategies of all groups on the Day 5 in MWM test. (f) The percentage of times spent in the each quadrant in all probe trials is shown at after EA. $^{*}P < 0.05$, $^{**}P < 0.01$, $^{***}P < 0.001$ versus the WT group; $^{\#}P < 0.05$, $^{\#\#}P < 0.01$ versus the APP/PS1 group; $^{\wedge}P < 0.05$, $^{\wedge\wedge}P < 0.01$ versus the APP/PS1 + Non-EA group. Each group, n = 10.

learning and memory and the platform was removed. Each mouse was allowed to swim freely for 90 s. The frequency that each mouse crossed the position where the platform was once placed and the time that it spent in the target quadrant were recorded.

To assess memory flexibility, 24 h following the probe trial, reversal platform training began. The hidden platform was placed into the center of the quadrant 180° from the original training location. Mice were released from one of four possible starting points and allowed to search for the hidden platform for a maximum of 90 s. If a mouse did not find the platform within 90 s, it would be removed from the water and placed on the platform for 15 s by researchers.

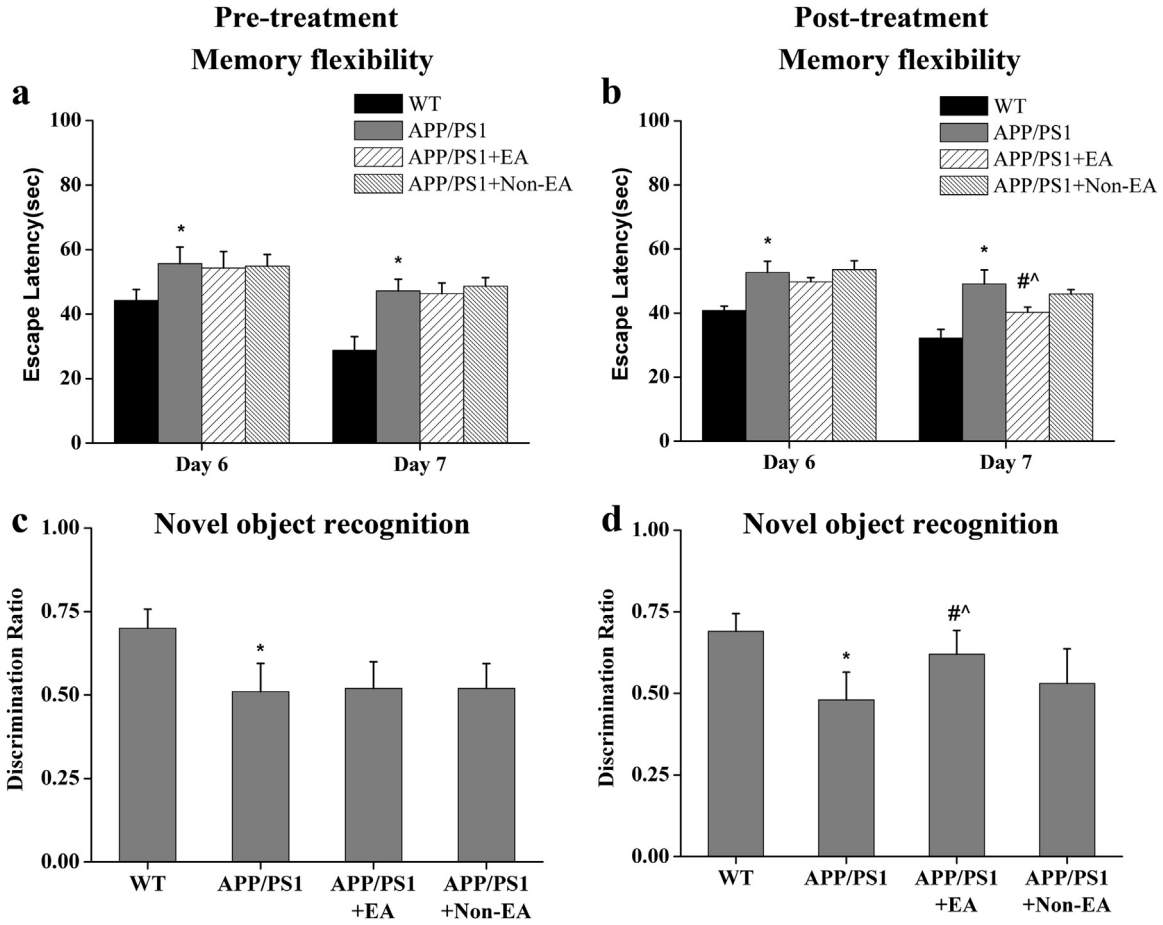

Fig. 3. EA improved memory flexibility and novel object recognition ability in the APP/PS1 mice. (a and b) The escape latency during the memory flexibility test at pre-treatment and post-treatment. (c and d) The discrimination ratio of novel object recognition at pre-treatment and post-treatment. $^{*}P < 0.05$ versus the WT group; $^{\#}P < 0.05$ versus the APP/PS1 group; $^{\wedge}P < 0.05$ versus the APP/PS1 + Non-EA group. Each group, n = 10.

2.5. Novel object recognition test

Novel object recognition was adapted from procedure described by Bevins and Besheer [31]. Each animal was allowed a 10 min training session with exposure to two identical, non-toxic objects (glass or hard plastic items) placed in the back left and right corners of the arena. After the training session, the animal was returned to its home cage for a 30-min retention interval. For testing, each animal was lowered into to the testing arena in which one familiar object was replaced with a novel object. The animal was lowered into the arena, equidistant and facing away from each object. Each session was video record and the animal was given 5 min to explore. The time spent exploring each object was scored for each mouse from the video. Exploration was defined as the animal's nose being within 2 cm of and pointed toward the object. Time during which the animal propped itself up on the object in order to explore higher levels of the arena was not considered exploration time for that object. The discrimination ratio was calculated as the time spent with the novel object divided by the total time spent exploring either object. Objects were randomized and counterbalanced across animals and groups. Objects and arenas were thoroughly cleaned with 70% ethanol between trials to prevent olfactory cues.

Of note, the visual ability of each mouse was assessed by suspending the animal by the tail and slowly lowering it toward a sold dark surface (a table) for three successive trials. Visual acuity was demonstrated by the animal's reaching for the surface before vibrissae made contact with it. All mice demonstrated full visual capability.

2.6. PET/CT scans

Before and after 4 weeks EA treatment, we randomly selected six or seven mice from each group for the PET/CT scans, the detection of ^{18}F-FDG combined with in-line PET/CT was performed, 12 h before scanning in mice (24, each set of 6, 28–32 g) fast, and in order to reduce or avoid the blood sugar concentration factors on ^{18}F-FDG metabolic distribution in the little mouse. Mice tail intravenous, blood sugar to normal range (7.0–10.1 tendency/L). Mice intraperitoneal injection of tracer (^{18}F-FDG dose of about 18.5 MBq). Mice after the injection of tracer placed inside the cage, let its free 40 min, 40 min later put the mice in the anesthesia induction box with gas anesthesia (made up of 5% isoflurane and 95% oxygen, about 5 min).

PET/CT scan: mice were received intraperitoneal injection of ^{18}F-FDG developer after about 40 min started collecting ^{18}F-FDG imaging head image, the mice in the Netherlands Milabs VeCTor + PET/SPECT/CT imaging system triad, scanning field contains the whole brain in mice and the neck, to adopt 3D model acquisition, image filter back projection reconstruction in mice axial surface, sagittal and coronal CT images were analyzed, and through PMOD software (PMOD Technologies, Zurich, Switzerland) with PET/CT image fusion, and through the Gaussian smooth 3 d (0.8 mm FWHM) filtering, and adjust the image color order to obtain high signal-to-noise ratio of images. Similar images are axial surface, sagittal and coronal plane coordinates the same cross section, by PMOD software analysis ^{18}F-FDG various brain regions in mice brain tissue uptake rate per gram.

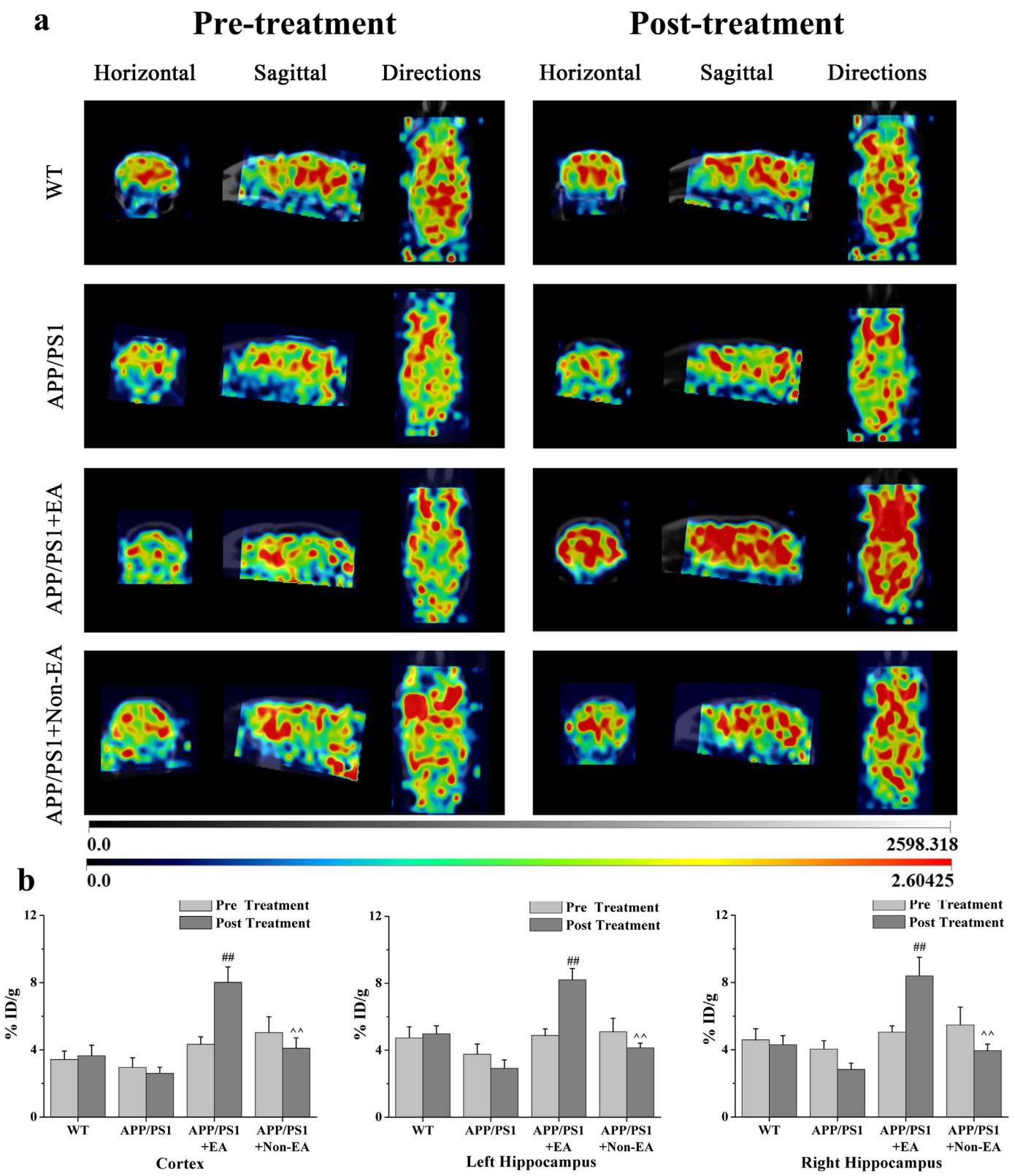

Fig. 4. Brain ^{18}F-FDG/PET images in APP/PS1 mice before and after EA treatment. (a) Glucose uptake in the brain regions at pre-treatment and post-treatment. The horizontal, sagittal images were showed and the directions were analyzed. (b) The percentage of glucose uptake (ID) than weight (g) (%). The data are presented as mean ± S.E.M from 6/7 individual mice. $^{\#\#}P < 0.01$ versus the APP/PS1 group; $^{\wedge\wedge}P < 0.01$ versus the APP/PS1 + Non-EA group.

2.7. Western blotting

We randomly selected five mice from each group for the protein experiment, protein was extracted from the hippocampus and cortex and homogenized in radio immunoprecipitation assay buffer (Thermo Fisher Scientific, USA). The protein concentration was determined using the bicinchoninic acid assay (Thermo Fisher Scientific, USA) and a total of 50 μg protein was separated by electrophoresis (90 V for

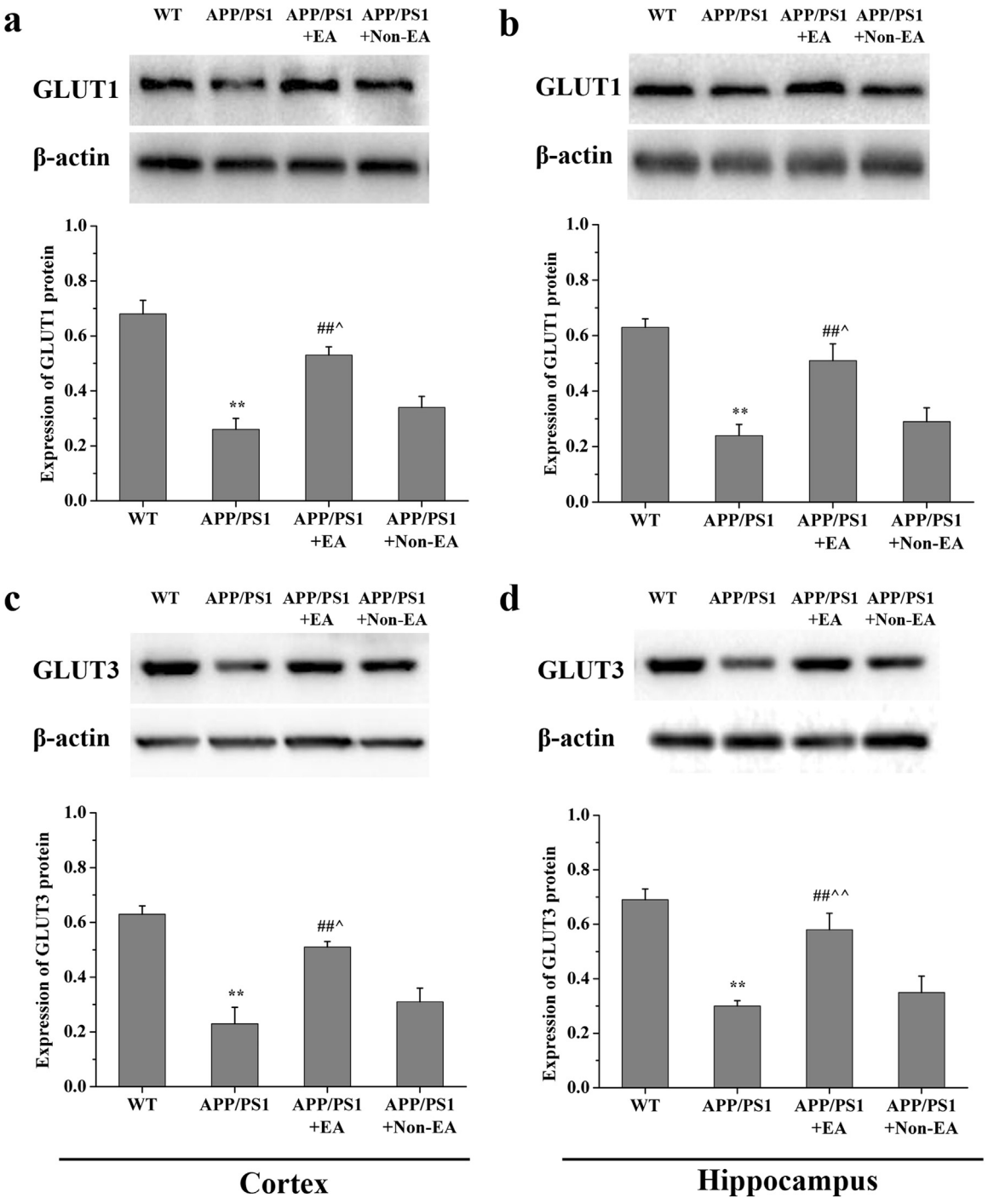

Fig. 5. The expression of GLUT1 and GLUT3. Representative immunoblots of GLUT1 and GLUT3 in the cortex and hippocampus in each group. The immunoreactivity of protein was normalized to β-actin. Experiments were repeated three times and individual data are presented as mean ± S.E.M. from 5 individual mice in each group. $^{**}P < 0.01$ versus the WT group; $^{\#\#}P < 0.05$ versus the APP/PS1 group; $^{\wedge}P < 0.05$, $^{\wedge\wedge}P < 0.01$ versus the APP/PS1 + Non-EA group.

30 min) on 10% SDS-PAGE gels (Bio-Rad Laboratories, Inc., Hercules, CA, USA). Proteins were transferred onto polyvinylidene fluoride membranes (EMD Millipore Billerica, MA, USA). The membranes were blocked for 2 h with 5% skimmed milk at room temperature and incubated with antibodies against Aβ (1:1000), Akt (1:1000), p-Akt (1:1000), GLUT1 (1:1000), GLUT3 (1:1000), mTOR (1:1000), p-mTOR (1:1000), AMPK (1:1000), p-AMPK (1:1000) and β-actin (1:5000) at 4 °C overnight and subsequently incubated with HRP-conjugated secondary antibody (1:5000) for 1 h. The protein bands were visualized with enhanced chemiluminescence and imaged with the Bio-Image Analysis system (Bio-Rad Laboratories, Inc.). The ratios of protein band intensities to β-actin were determined.

2.8. Thioflavin staining

We randomly selected five mice from each group for the histology experiment. The brain tissues were fixed with 4% paraformaldehyde and embedded in paraffin and the subsequent histological procedures. Thioflavin staining (ThS) was developed in sections mounted on paraffin-coated slices. After rehydration in ethanol and xylene solution, slices were incubated in 0.3% potassium permanganate, 1% Oxalic acid, and 1% sodium borohydride in order, 5 min each time. Next,

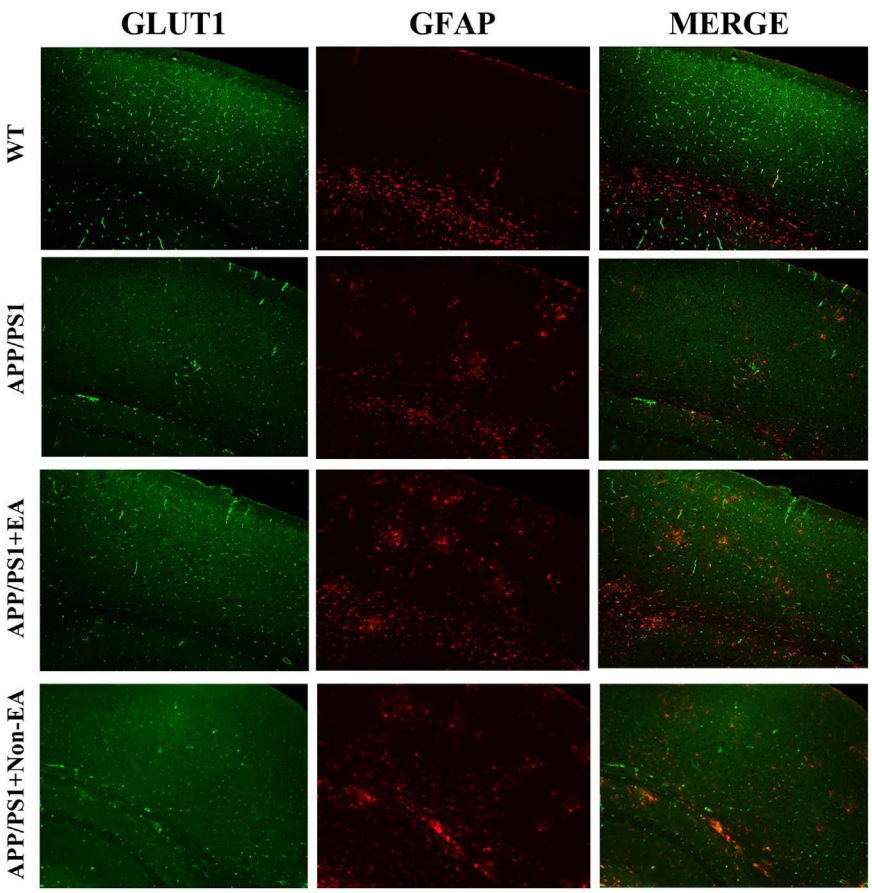

Fig. 6. The co-expression of GLUT1 and GFAP in cortex. Representative immunofluorescence of GLUT1 and GFAP in the cortex in each group. GLUT1-positive cells are green. GFAP-positive cells are red. GLUT1 and GFAP double-positive cells are yellow. Experiments were repeated three times and individual data are presented as mean ± S.E.M. from 5 individual mice in each group. Scale bar 100 μm. (For interpretation of the references to color in this figure legend, the reader is referred to the web version of this article.)

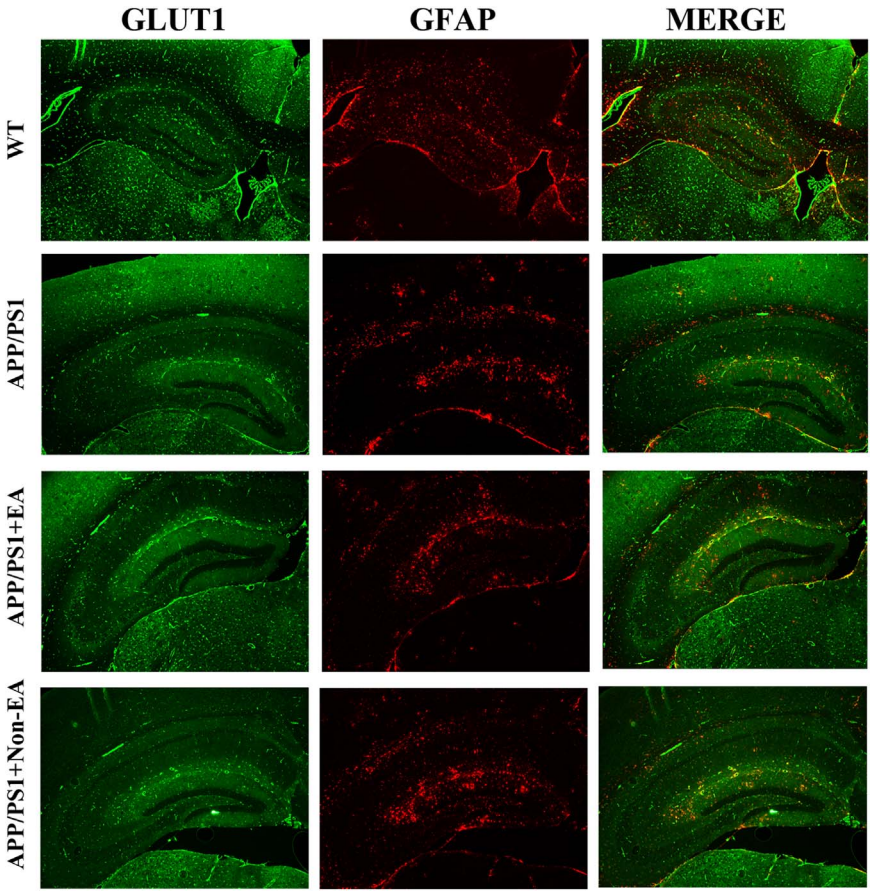

Fig. 7. The co-expression of GLUT1 and GFAP in hippocampus. Representative immunofluorescence of GLUT1 and GFAP in the hippocampus in each group. GLUT1-positive cells are green. GFAP-positive cells are red. GLUT1 and GFAP double-positive cells are yellow. Experiments were repeated three times and individual data are presented as mean ± S.E.M. from 5 individual mice in each group. Scale bar 200 μm. (For interpretation of the references to color in this figure legend, the reader is referred to the web version of this article.)

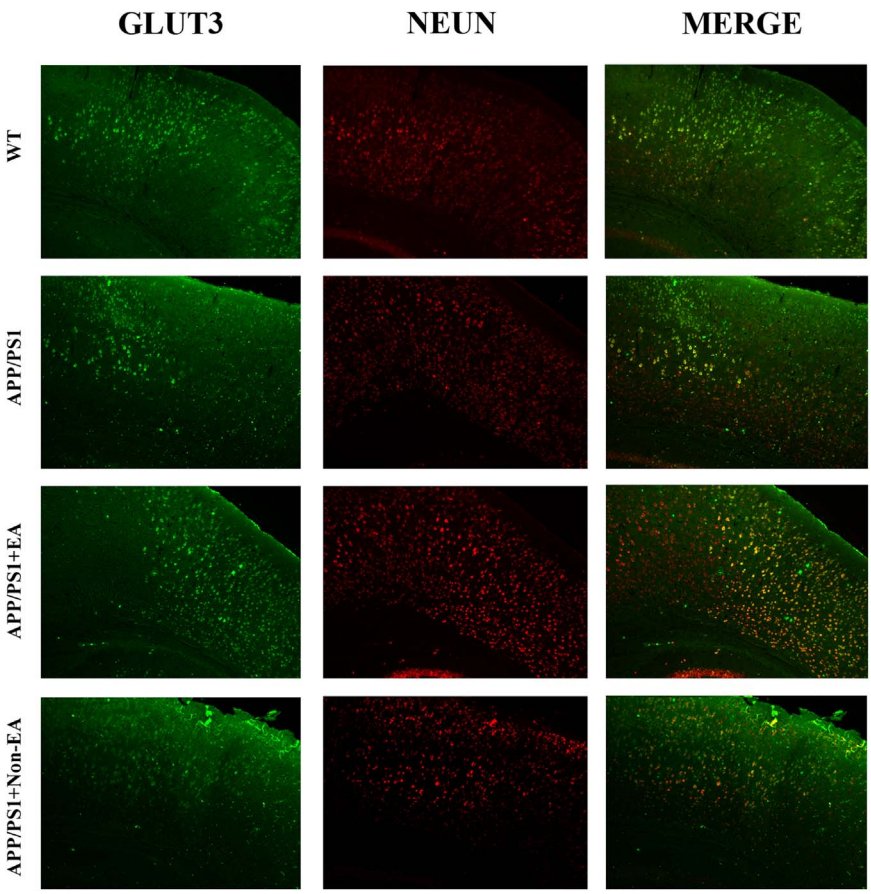

Fig. 8. The co-expression of GLUT3 and NeuN in cortex. Representative immunofluorescence of GLUT3 and NeuN in the cortex in each group. GLUT3-positive cells are green. NeuN-positive cells are red. GLUT3 and NeuN double-positive cells are yellow. Scale bar 100 μm. (For interpretation of the references to color in this figure legend, the reader is referred to the web version of this article.)

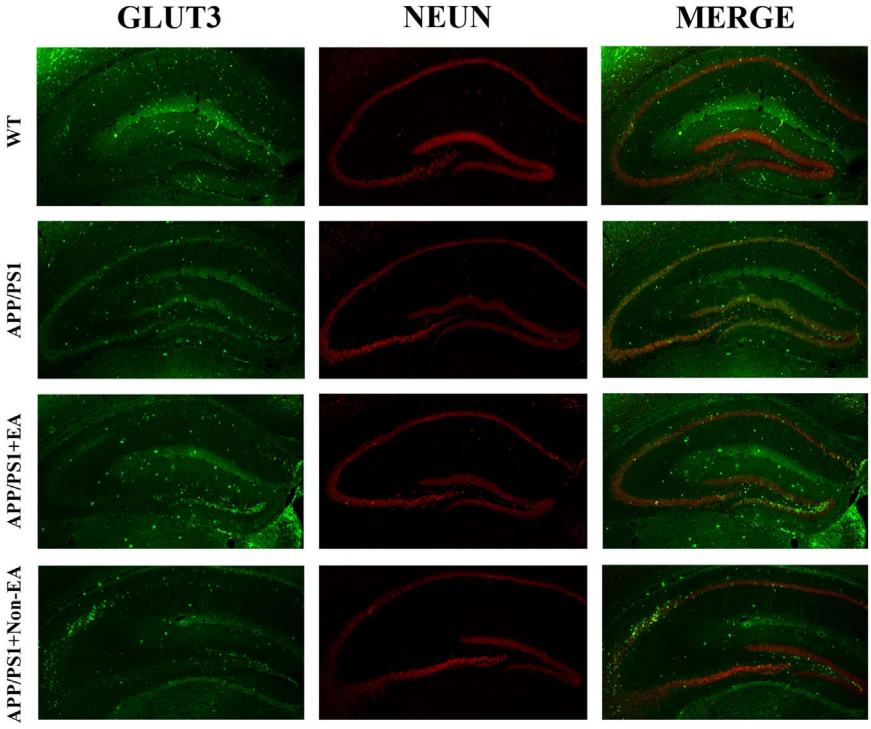

Fig. 9. The co-expression of GLUT3 and NeuN in hippocampus. Representative immunofluorescence of GLUT3 and NeuN in the hippocampus in each group. GLUT3-positive cells are green. NeuN P-positive cells are red. GLUT3 and NeuN double-positive cells are yellow. Scale bar 200 μm. (For interpretation of the references to color in this figure legend, the reader is referred to the web version of this article.)

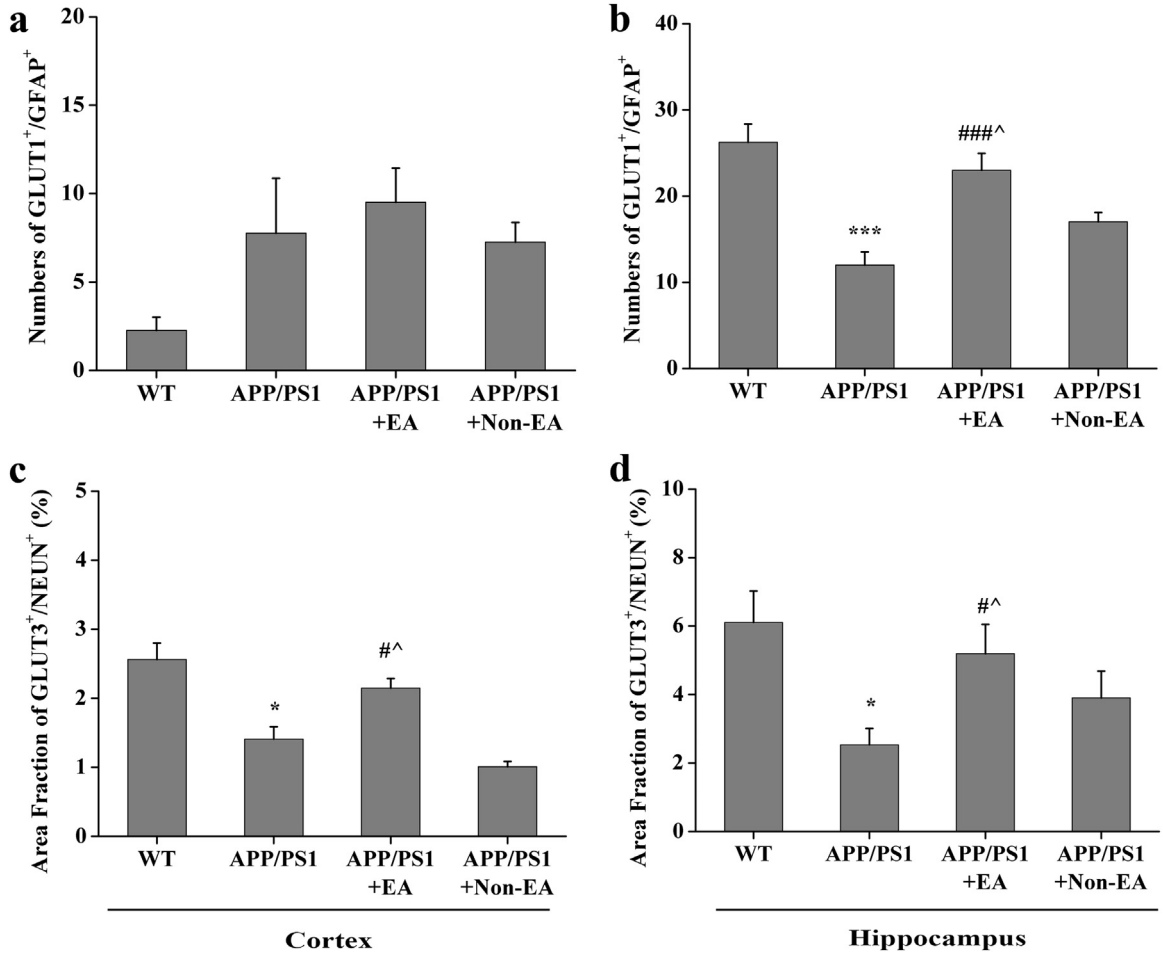

Fig. 10. The statistics of GLUT1/GFAP and GLUT3/NeuN co-expression. (a and b) GLUT1 and GFAP double-positive cells were analyzed in cortex and hippocampus. (c and d) GLUT3 and NeuN double-positive cells were analyzed in cortex and hippocampus. Experiments were repeated three times and individual data are presented as mean ± S.E.M. from 5 individual mice in each group.

immersed slices in the 0.0125% ThS solution (Sigma, USA) for 8 min in dark. Then, slices were washed twice in 50% ethanol for 5 min and coverslipped with antifade mounting medium in dark. Ths staining of hippocampus was observed by fluorescence microscopy (Nikon TS100, Japan).

2.9. Immunohistochemistry and immunofluorescence staining

Immunohistochemistry (IHC) was performed on the 5 μm-thick coronal paraffin sections. Aβ (1-42) levels were examined with DAB kits according to the manufacturer's protocols. The sections were incubated in 3% hydrogen peroxide and normal serum at 37 °C for 10 min to block the non-specific protein binding. Sections were incubated with primary anti-Aβ(1-42) antibody (1:200) at 4 °C overnight and subsequently incubated with secondary antibody. Aβ(1-42)-positive cells were stained brown and hematoxylin was used to visualize the nuclei of all cells. Images of Aβ(1-42) deposition in the cortex and hippocampus were captured using an optic microscope (DFC310 FX; Leica Microsystems, Inc., Buffalo Grove, IL, USA) and analyzed with an image analysis system (Image-Pro Plus, version 6.0; Motic China Group Co., Ltd., Xiamen, China). The density of Aβ (1-42) deposition (the percentage of positively-stained brown cells) was determined by subtracting the background density and non-specific binding. The software was used to perform the semi-quantitative evaluation.

Immunofluorescence (IF) staining was performed on the 5 μm-thick coronal paraffin sections. The slices were incubated overnight at 4 °C with the primary antibodies anti-GLUT1 (dilution of 1:200), anti-GLUT3 (dilution of 1:200), anti-GFAP (dilution of 1:1000) and anti-NeuN (dilution of 1:1000), and anti-MAP2 (dilution of 1:500), then incubated with secondary antibodies conjugated to fluorophores Alexa Fluor 488 (dilution of 1:200, A21441, Life Technologies, USA), Alexa Fluor 546 (dilution of 1:200, A10036, Life Technologies, USA) for 2 h at room temperature in the dark, respectively. Nuclei of all cells were counterstained with DAPI (dilution of 1:1000; Santa Cruz, USA). The tissue slides were mounted in mounting medium (Vector Laboratories, USA) and images were captured using a confocal fluorescence microscope (LSM710, Carl Zeiss, Germany). The average number of double-labeled positive cells from three slices for each rat with six fields of view/slice was used for statistical analysis.

2.10. Enzyme-linked immunosorbent assay (ELISA)

Aβ (1-42) in cortex and hippocampus were measured by ELISA kits according to the manufacturer's instructions (Xitang, Shanghai, China). Briefly, the wells were coated with 100 μl capture antibody at 4 °C. Followed three washes, using 200 μl assay diluents to block at room temperature for 1 h, then 100 μl diluted Aβ (1-42) standards and test samples were added and incubated for 1 h at 37 °C. Following repeated washes, every well was added with the substrate and incubated for 20 min at room temperature, and then the absorbance was quantitated by using an ELISA reader (BioTek, Model ELX800, USA) at 450 nm according to Aβ (1-42) protein standards.

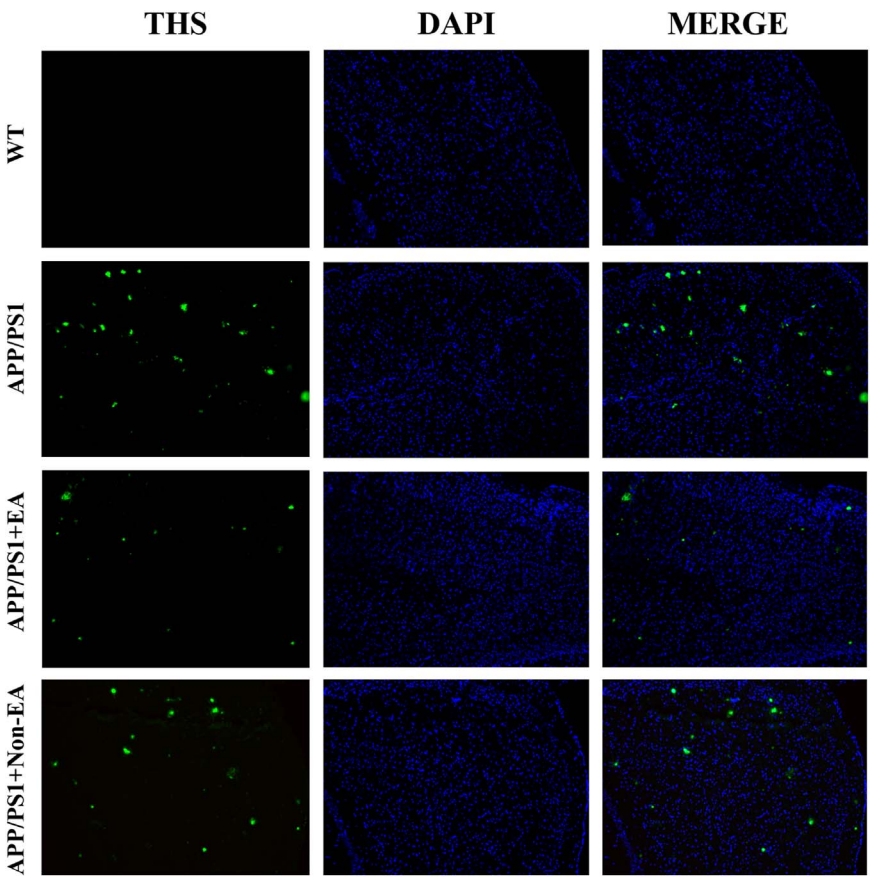

Fig. 11. The Ths-Aβ deposition in cortex. Representative staining of Ths-Aβ deposition in the cortex in each group. Ths-Aβ-positive cells are green. Nuclei counterstained with DAPI (blue). Scale bar 100 μm. (For interpretation of the references to color in this figure legend, the reader is referred to the web version of this article.)

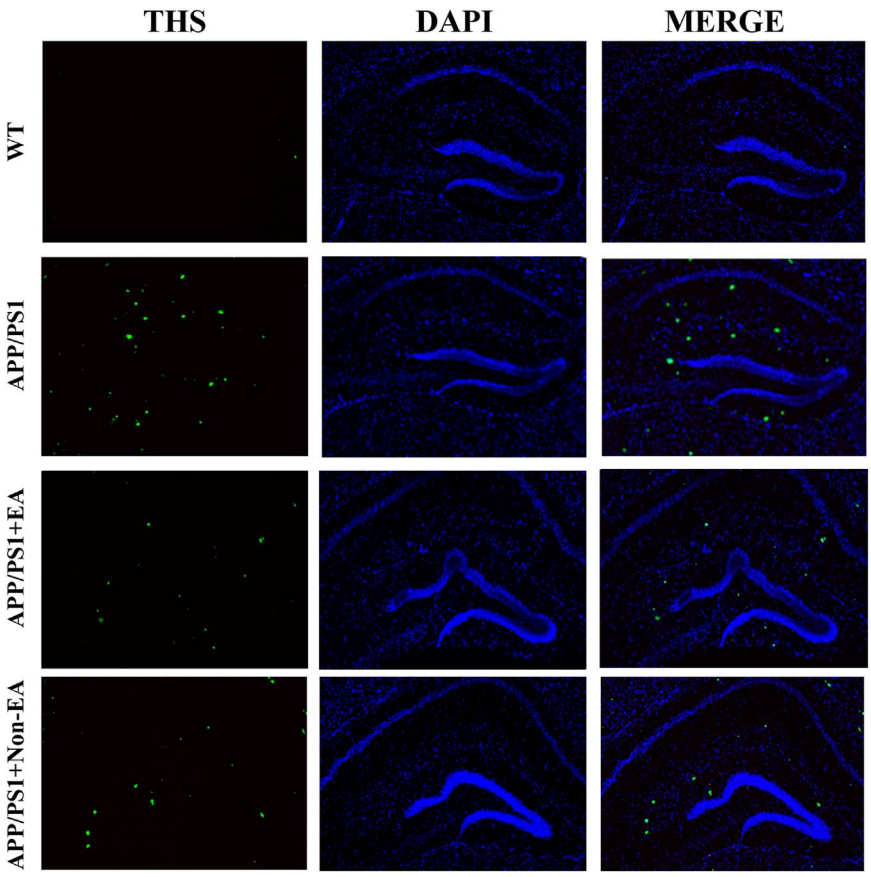

Fig. 12. The Ths-Aβ deposition in hippocampus. Representative staining of Ths-Aβ deposition in the hippocampus in each group. Ths-Aβ-positive cells are green. Nuclei counterstained with DAPI (blue). Scale bar 200 μm. (For interpretation of the references to color in this figure legend, the reader is referred to the web version of this article.)

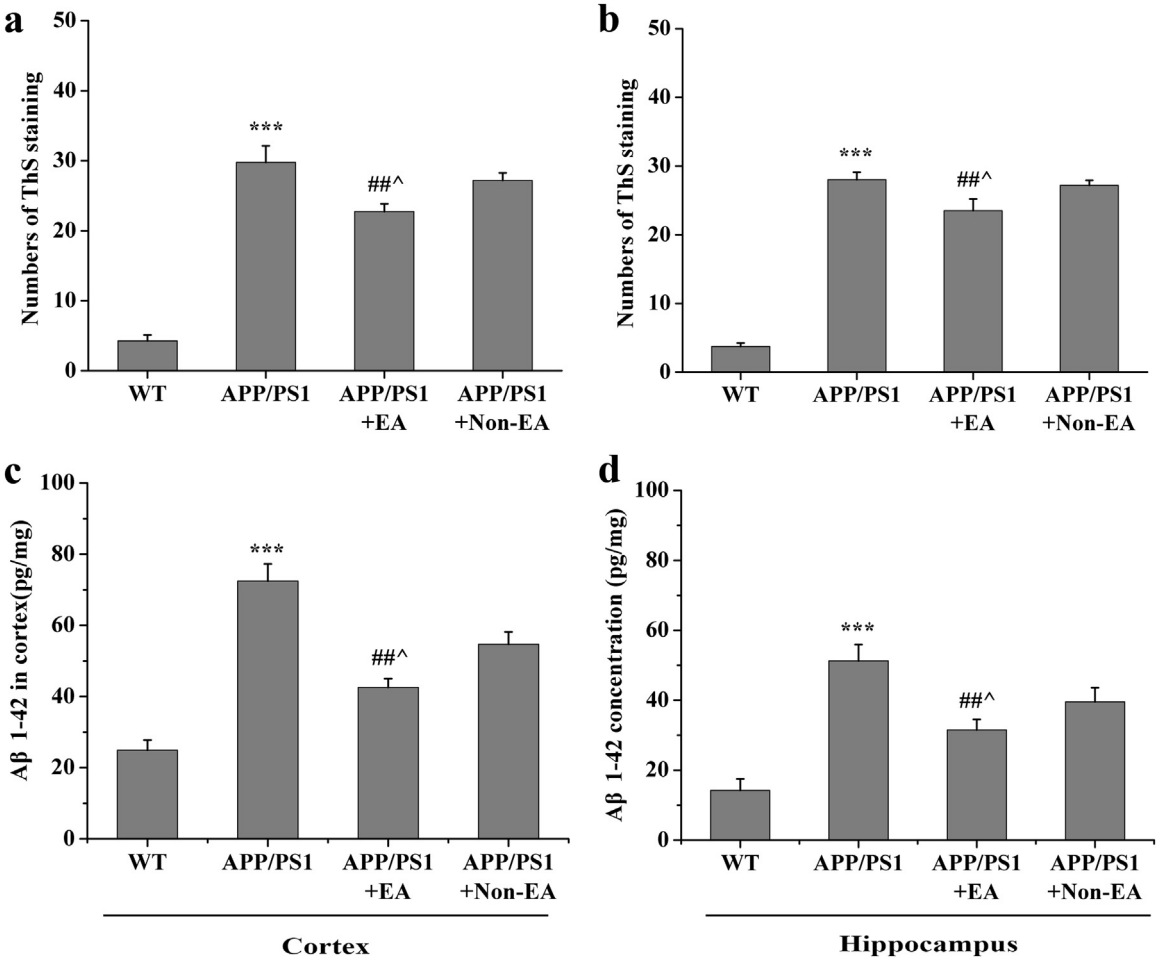

Fig. 13. The staining of Aβ deposition. (a and b) The number of Ths-Aβ deposition were analyzed in the cortex and hippocampus. (c and d) The expression of Aβ (1-42) were analyzed by ELISA in the cortex and hippocampus. Experiments were repeated three times and individual data are presented as mean ± S.E.M. from 5 individual mice in each group. $^{***}P < 0.001$ versus the WT group; $^{\#\#}P < 0.01$ versus the APP/PS1 group; $^{\wedge}P < 0.05$ versus the APP/PS1 + Non-EA group.

2.11. Statistical analysis

The results for each group are expressed as the means ± S.E.M. The latency performance was analyzed using repeated measures analysis of variance (RM-ANVOA) across days. Probe trial time in target quadrant as compared to time in the other quadrants and the times of passing the hidden platform position, PET data, discrimination ratio of novel object recognition, western blot, thioflavin staining, immunohistochemistry and immunofluorescence staining results were analyzed by one-way ANOVA and comparisons between groups were made by Fisher's least significant difference (LSD) or Games-Howell test. The significance level was set at $^{*}P < 0.05$ or $^{**}P < 0.01$ or $^{***}P < 0.001$ in two-way comparisons.

3. Results

3.1. EA ameliorated cognitive impairments in APP/PS1 mice

The effects of before and after EA treatment on the spatial reference learning and memory and memory flexibility and novel object recognition ability were evaluated. In the place navigation trials, navigation paths of training provided evidence that the APP/PS1 + EA group presented strategies before and after EA treatment that were more similar to the WT group than the APP/PS1 + Non-EA group and the APP/PS1 group (tracing paths was not shown before and after EA). As shown in Fig. 2a and b, the escape latency in all groups had shown a downward trend before and after EA treatment, and before EA treatment, it had no differences during the APP/PS1 + EA group, the APP/PS1 + Non-EA group and the APP/PS1 group ($p > 0.05$, at the Day 4 in Fig. 2a). However, after EA treatment, the APP/PS1 + EA group showed better spatial reference learning performance (shorten the escape latency) than the APP/PS1 + Non-EA group and the APP/PS1 group ($F_{(3, 36)} = 35.352$, $p < 0.001$, at the Day 4 in Fig. 2b). During the probe trial, before EA treatment, the times of passing the hidden platform position had no differences during the APP/PS1 + EA group, the APP/PS1 + Non-EA group and the APP/PS1 group before EA treatment ($p > 0.05$, Fig. 2c). After EA treatment, the representative navigation paths at the last day of testing showed that the frequency of passing the hidden platform position was increased in the APP/PS1 + EA group compared with the APP/PS1 + Non-EA group and the APP/PS1 group ($F_{(3,36)} = 24.810$, $p < 0.001$, Fig. 2d and e). Simultaneously, it showed that the APP/PS1 + EA group spent more time in the target quadrant compared to the other quadrants than the APP/PS1 + Non-EA group and the APP/PS1 group ($F_{(3,36)} = 36.678$, $p < 0.001$, Fig. 2f). During the memory flexibility test, before EA treatment, it had no differences during the APP/PS1 + EA group, the APP/PS1 + Non-EA group and the APP/PS1 group ($p > 0.05$, Fig. 3a). However, after EA treatment, the APP/PS1 + EA group showed shorten the escape latency than the APP/PS1 + Non-EA group and the APP/PS1 group ($F_{(3, 36)} = 64.185$, $p < 0.001$, Fig. 3b). When mice were exposed to the novel object recognition test before EA treatment, the WT group spent more time with the novel object than the familiar one, no significant group differences were detected for object discrimination during the APP/PS1 + EA group, the APP/PS1 + Non-EA group and the APP/PS1 group ($p > 0.05$,

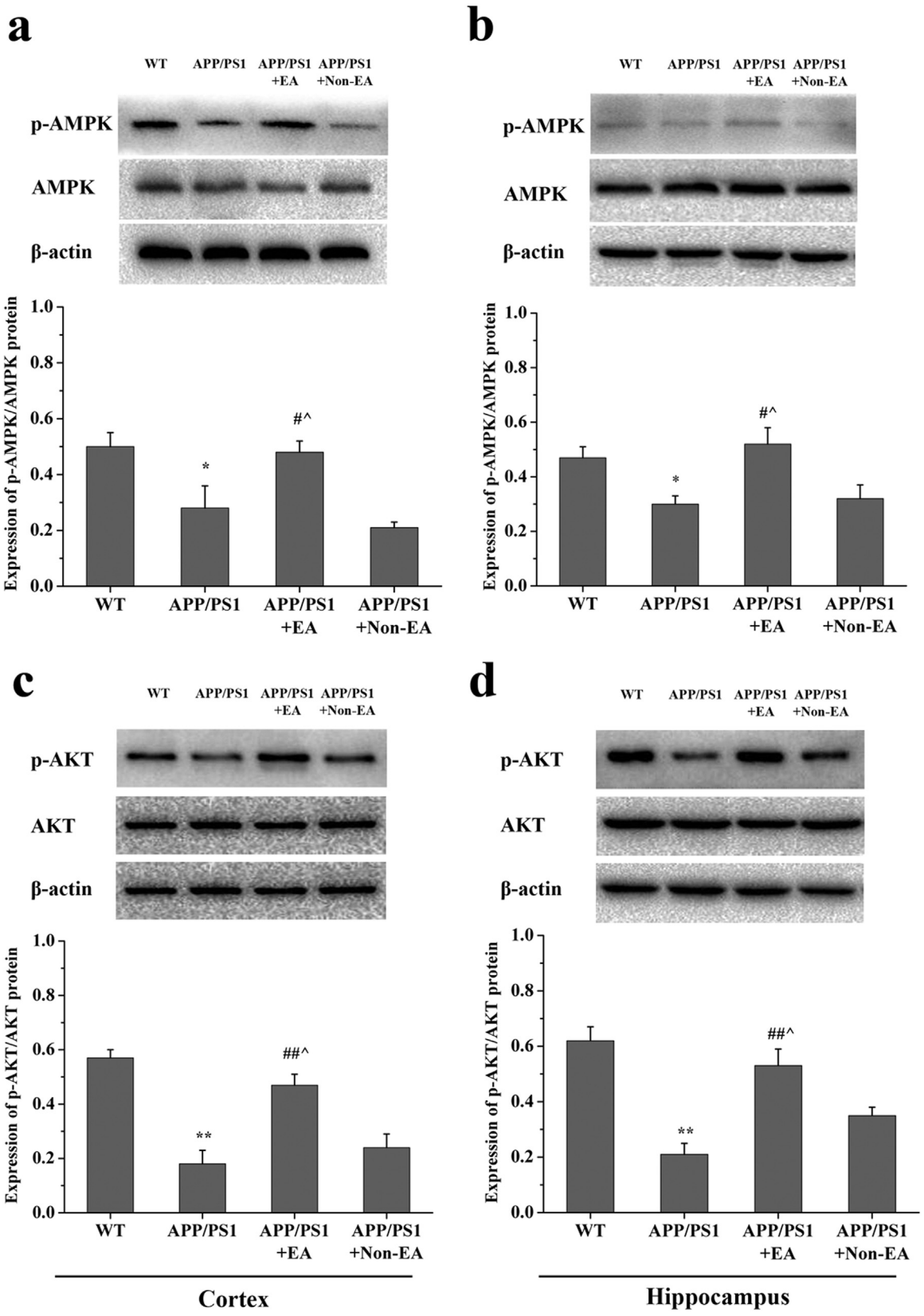

Fig. 14. The phosphorylation of AMPK and AKT. Representative immunoblots of total p-AMPK, p-AMPK, p-mTOR and mTOR in the cortex and hippocampus in each group. The immunoreactivity of protein was normalized to β-actin. The results are expressed as arbitrary units (phosphorylated protein/total protein). Experiments were repeated three times and individual data are presented as mean ± S.E.M. from 5 individual mice in each group. $^{*}P < 0.05$, $^{*}P < 0.01$ versus the WT group; $^{\#}P < 0.05$, $^{\#\#}P < 0.01$ versus the APP/PS1 group; $\hat{}P < 0.05$ versus the APP/PS1 + Non-EA group.

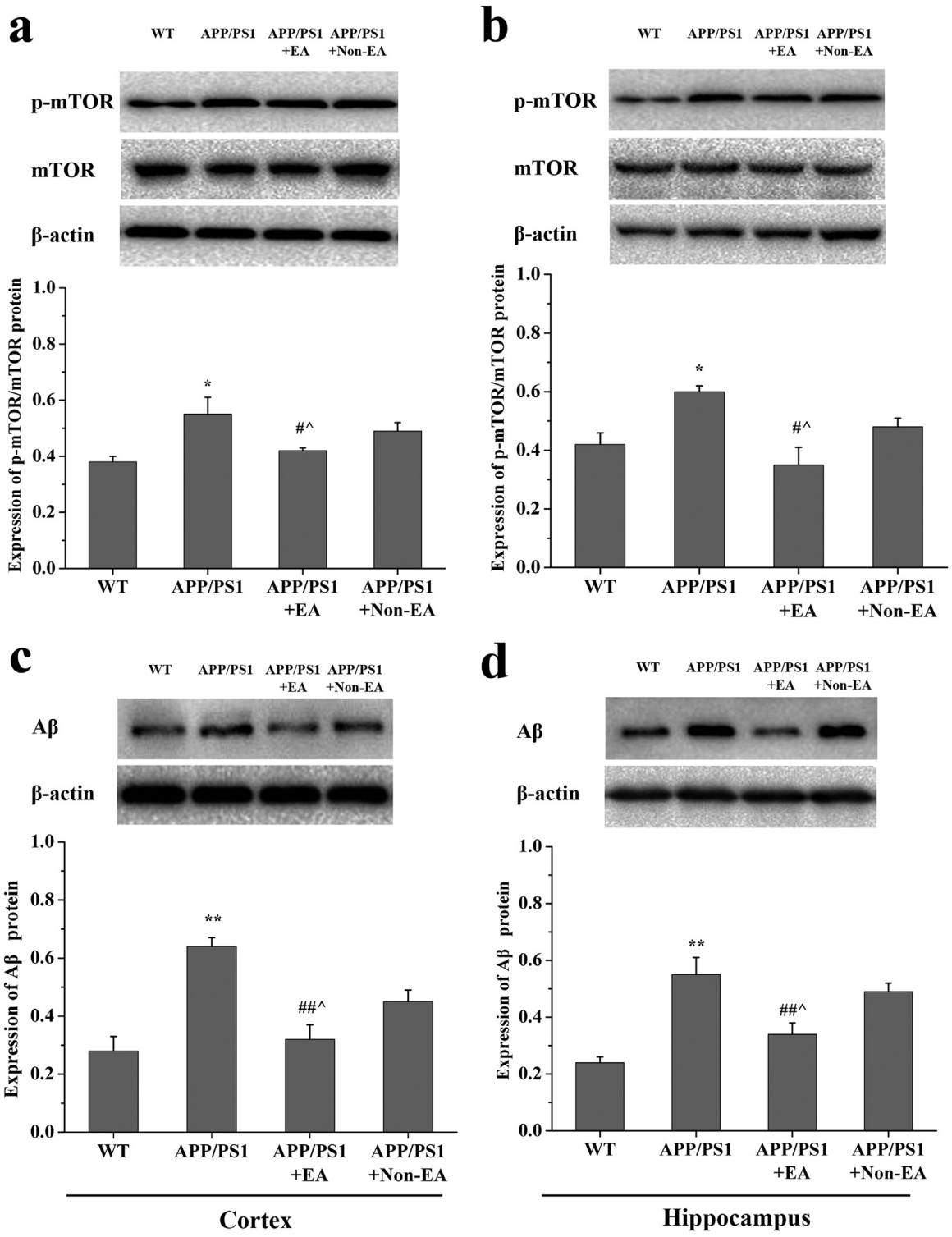

Fig. 15. The expression of mTOR and Aβ (1-42). Representative immunoblots of p-mTOR, mTOR and Aβ (1-42) in the cortex and hippocampus in each group. The immunoreactivity of protein was normalized to β-actin. The results are expressed as arbitrary units (phosphorylated mTOR/total mTOR and Aβ (1-42)/β-actin). Experiments were repeated three times and individual data are presented as mean ± S.E.M. from 5 individual mice in each group. $^{*}P < 0.05$, $^{**}P < 0.01$ versus the WT group; $^{\#}P < 0.05$, $^{\#\#}P < 0.05$ versus the APP/PS1 group; $^{\wedge}P < 0.05$ versus the APP/PS1 + Non-EA group.

Fig. 3c). However, after EA treatment, the APP/PS1 + EA group explored more time with the novel object, thus their discrimination ratio increased compared with the APP/PS1 + Non-EA group and the APP/PS1 group ($F_{(3,36)} = 8.931, p < 0.001$, Fig. 3d). These results suggested that EA treatment obviously attenuated the cognitive impairments in APP/PS1 mice.

3.2. EA increased brain glucose metabolism in APP/PS1 mice

^{18}F-FDG images were recorded in all groups by in-line PET/CT imaging system. Nineteen cerebral regions were analyzed of glucose metabolism in mice, including the left and right hippocampus, the left and right amygdala, the cortex, and the cingulate gyrus. Using the same color standard and color code from high to low showing glucose

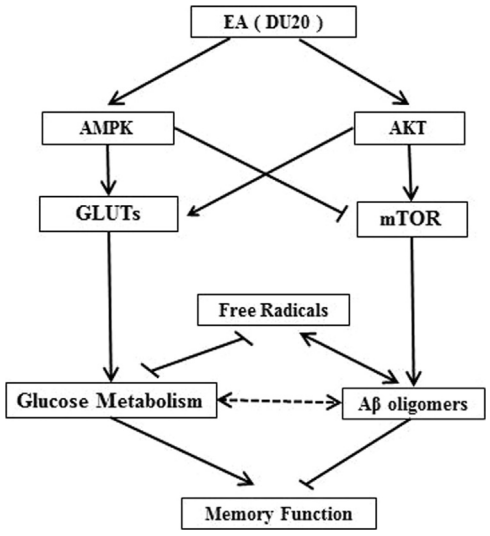

Fig. 16. AMPK and AKT in EA-induced energy metabolism. AMPK and AKT were activated by EA treatment, further triggered GLUTs to increase the energy metabolism, and negatively regulated mTOR to induce autophagy and eliminate Aβ deposition.

metabolism, the result showed that the glucose uptake of all brain regions had no differences during the four groups before EA treatment ($p > 0.05$, Supplementary Table 1). However, after EA treatment, the glucose uptake of the cingulate gyrus and the cerebellum regions in the APP/PS1 group were significantly decreased compared with the WT group (Supplementary Table 1), and an increase of glucose uptake tin the right hippocampus, the left hippocampus, the cortex, the cingulate gyrus, the basal forebrain septum, the brain stem, and the cerebellum regions displayed in the APP/PS1 + EA group compared with the APP/PS1 + Non-EA group and the APP/PS1 group ($F_{(3, 21)} = 5.301$, $p < 0.001$, $F_{(3, 21)} = 10.825$, $p < 0.001$, $F_{(3, 21)} = 14.081$, $p < 0.001$,Fig. 4a and b, Supplementary Table 1). Whereas the glucose uptake of the left amygdala and the right amygdala regions had no difference in the APP/PS1 + EA group compared with the APP/PS1 + Non-EA group and the APP/PS1 group ($p > 0.05$, Supplementary Table 1). These results suggested that EA treatment markedly increased the glucose metabolism of the cortex and hippocampus in APP/PS1 mice.

3.3. EA increased the expression of GLUT1 and GLUT3 in APP/PS1 mice

Since EA could increase the glucose metabolism of the hippocampus, the cortex, the cingulate gyrus, and cerebellum regions, the learning and memory-related two regions that include the hippocampus and cortex [32,33] were selected for revealing whether EA affects the activation of GLUT1 and GLUT3 after EA treatment. The results showed that the expression of GLUT1 and GLUT3 were significantly decreased in the hippocampus and cortex in the APP/PS1 group compared with the WT group, however, after EA treatment, an increase of the expression of GLUT1 and GLUT3 displayed in the hippocampus and cortex of the APP/PS1 + EA group compared with the APP/PS1 + Non-EA group and the APP/PS1 group ($F_{(3, 16)} = 7.369$, $p < 0.001$, and $F_{(3, 16)} = 12.569$, $p < 0.001$, $F_{(3, 16)} = 14.582$, $p < 0.001$, $F_{(3, 16)} = 9.658$, $p < 0.001$, Fig. 5a, b, c and d). Furthermore, dual labeling of GLUT1 and GFAP, GLUT3 and NeuN were used to determine whether the increase of glucose metabolism occurred in neurons or non-neuronal cells. The results showed that the co-expressions of GLUT1 and GFAP, GLUT3 and NeuN occurred in each group (Figs. 6–9), and they were increased in the cortex of the APP/PS1 + EA group compared with the APP/PS1 + Non-EA group and the APP/PS1 group ($F_{(3, 16)} = 19.148$, $p < 0.001$, Fig. 10c), and they were increased in the hippocampus of the APP/PS1 + EA group compared with the APP/PS1 + Non-EA group and the APP/PS1 group ($F_{(3, 16)} = 14.604$, $p < 0.001$, $F_{(3, 16)} = 17.996$, $p < 0.001$, Fig. 10b and d). Additionally, the results showed that the dual labeling of GLUT1 and NeuN, GLUT1 and MAP2, GLUT3 and GFAP respectively did not co-location in each group (Supplementary Figs. S1 and S2). These results suggested that GLUT1 expressed in GFAP-positive glial cell, and GLUT3 expressed in neuron, and EA-increased energy metabolism occurred in neurons or non-neuronal cells.

3.4. EA delayed the Aβ (1-42) deposition of hippocampus and cortex in APP/PS1 mice

The expression of Aβ (1-42) in the cortex and hippocampus of APP/PS1 mice were quantified by thioflavin (ThS) staining. The APP/PS1 group showed a significant increase in Ths-Aβ deposition in the cortex and hippocampus than that of the WT group, however, after EA treatment, the Ths-Aβ deposition of the APP/PS1 + EA group was decreased in the cortex and hippocampus compared with the APP/PS1 + Non-EA group and the APP/PS1 group ($F_{(3, 16)} = 61.425$, $p < 0.001$, $F_{(3, 16)} = 111.084$, $p < 0.001$, Figs. 11–13). Moreover, the levels of Aβ (1-42) were quantified by western blot and ELISA and showing in line with the results of ThS-Aβ deposition ($F_{(3, 16)} = 8.597$, $p < 0.001$, $F_{(3, 16)} = 13.024$, $p < 0.001$, Fig. 15c and d, Supplementary Fig. S3). These results suggested that EA treatment could delay the Aβ deposition of cortex and hippocampus in APP/PS1 mice.

3.5. EA increased the expression of AMPK and AKT in APP/PS1 mice

The results showed that the ratios of p-AMPK/total-AMPK and p-AKT/total-AKT were significantly decreased in the cortex and hippocampus in the APP/PS1 group compared with the WT group (Fig. 14a, b, c and d), however, after EA treatment, an increase of the ratios of p-AMPK/total-AMPK and p-AKT/total-AKT displayed in the cortex and hippocampus of the APP/PS1 + EA group compared with the APP/PS1 + Non-EA group and the APP/PS1 group ($F_{(3, 16)} = 5.254$, $p < 0.001$, $F_{(3, 16)} = 9.069$, $p < 0.001$, $F_{(3, 16)} = 10.257$, $p < 0.001$, $F_{(3, 16)} = 16.339$, $p < 0.001$, Fig. 14a, b, c and d). These results suggested that EA treatment increased the phosphorylation of AMPK and AKT in cortex and hippocampus in APP/PS1 mice.

3.6. EA modulated the expression of mTOR in APP/PS1 mice

The ratio of p-mTOR/total-mTOR were significantly increased in the cortex and hippocampus in the APP/PS1 group compared with the WT group (Fig. 15a and b). However, after EA treatment, an decrease of the ratio of p-mTOR/total-mTOR displayed in the cortex and hippocampus of the APP/PS1 + EA group compared with the APP/PS1 + Non-EA group and the APP/PS1 group ($F_{(3, 16)} = 6.201$, $p < 0.001$, $F_{(3, 16)} = 8.158$, $p < 0.001$, Fig. 15a and b). These results suggested that EA treatment increased the phosphorylation of mTOR in cortex and hippocampus in APP/PS1 mice.

4. Discussion

The APP/PS1 double transgenic mouse is characterized by Alzheimer's disease-like Aβ burden. It expresses a mutated allele of the human APP and PS1 genes, which induce Aβ plaque deposition in the brain at 6–7 months after birth [34] and cause memory deficits at 9 months after birth [35,36]. Therefore, in order to evaluate the effect of EA on cognitive impairment, the 9-month-old APP/PS1 mice were chosen. The present study demonstrated that low-frequency (1/20 Hz) EA at the DU 20 acupoint for four weeks obviously increased glucose metabolism particularly in the cortex and hippocampus regions in APP/PS1 mice, accompanied by cognitive improvement in spatial reference learning and memory and memory flexibility and novel object recognition performances. Further, we found metabolic homeostatic factors critical for glucose metabolism. These included phosphorylated

AMPK and AKT serine/threonine kinase. Simultaneously, EA-induced phosphorylated AMPK and AKT inhibited the phosphorylation level of the mTOR to decrease the accumulation of Aβ in the cortex and hippocampus of APP/PS1 mice.

EA, a complementary and alternative medicine treatment, is endorsed the World Health Organization and the National Institute of Health [37], which has been shown to improve cognitive deficits in clinical studies [38,39]. The study found that EA treatment at the DU 20 acupoint for four weeks could improve the spatial reference learning and memory performance in APP/PS1 mice, which is consistent with previously reported results in several animal models of AD [6,7,40,41]. Moreover, EA also improved the memory flexibility and novel object recognition ability in APP/PS1 mice. These suggest that EA could delay cognitive decline in particular with learning and memory in AD model mice.

Further, a number of epidemiological and functional neuroimaging studies have shown that the dysregulation of energy metabolism in the brain is a significant causative factor in the development of AD [42,43]. On the whole, most investigations of amyloidosis models have revealed unchanged [44,45] or decreased uptake [16–18]. Using small animal ^{18}F-FDG imaging, the present study found that the glucose metabolism of seventeen regions had no changes, including the right hippocampus, the left hippocampus, the cortex, the cingulate gyrus, the basal forebrain septum, the brain stem, the left amygdala, the right amygdala and the cerebellum regions, whereas the cingulate gyrus and the cerebellum regions were decreased in APP/PS1 transgenic mice. However, after EA treatment the glucose metabolism of seventeen regions were obviously increased, including the right hippocampus, the left hippocampus, the cortex, the cingulate gyrus, the basal forebrain septum, the brain stem, and the cerebellum regions, whereas the left amygdala and the right amygdala regions had no changes. Similar to previous studies, in the clinical randomized controlled trials (RCTs) of EA or acupuncture on stroke patients or migraines' patients or vascular dementia patients, the regional glucose metabolism were increased following EA by evaluation of ^{18}F-FDG/PET imaging [46–48]. In the animal experiments of EA or acupuncture on AD rats or SAMPS mouse, the ^{18}F-FDG/PET imaging revealed that treatment of EA can increase the uptake rate of glucose in hippocampus of SAMP8 mouse [49], and hippocampal and temporal regions of AD rats [50,51]. The presence of glucose transport proteins (GLUTs) is essential to supply glucose to the neurons and glia within the brain, for example, GLUT1 presents in astrocytes, and GLUT3 expresses in neurons [52]. The study demonstrated that EA could increase the expression of GLUT1 and GLUT3. Simultaneously, EA increased the co-location of GLUT1/GFAP and GLUT3/NeuN, and also found that the dual labeling of GLUT1/NeuN, GLUT1/MAP2 and GLUT3/GFAP did not co-location. These results suggested that EA increased GLUTs expression to improve energy metabolism of neurons or non-neuronal cells in cortex and hippocampus in AD model mice.

Studies have been suggested AMPK as a molecular hub for cellular energy metabolic control and presents highly throughout the brain where shown to be acted via direct phosphorylation of metabolic enzymes, and regulation of the GLUTs gene expression, and negatively regulation of the mTOR signaling in response to reduction of intracellular energy levels [53–55]. AKT plays a highly conserved role in the regulation of cellular energy metabolism, and positively regulates the mTOR signaling [56]. Accumulating evidence show that a disturbance in AMPK and AKT function have been implicated in neurodegenerative diseases such as AD [56,57]. Therefore, recent evidences suggest that AMPK and AKT is emerging as a potential therapeutic target for these neurodegenerative diseases. For example, metformin is a first-line diabetes drug and an activator of AMPK, which ameliorates AD-like pathology and memory declines in mice [58], and central acylated ghrelin improves hippocampal AMPK activation and partly reverses the impairment of energy and glucose metabolism in rats infused with Aβ [59]. Selenomethionine is able to reduce Aβ deposition, and markedly improve cognitive functions in triple transgenic AD mice through the PI3K/AKT signaling pathway [60]. The study demonstrated that EA increased AMPK expression in cortex and hippocampus which improved these regional glucose metabolism and memory impairments. Interestingly, we found that mTOR expression was decreased in cortex and hippocampus in response to negatively regulation of AMPK and positively regulation of AKT signaling. Therefore, it is concluded that AMPK function plays a more important role than AKT in EA-induced energy metabolism.

In addition, a number of mTOR-dependent and independent autophagy modulators have been identified to have positive effects in AD treatment [61]. The mTOR inhibition triggers autophagy to decrease Aβ and senile plaques and improve AD mouse memory impairment [62,63]. In fact, it is well-recognized that AMPK/mTOR signaling intersects with AD pathology in several aspects, suggesting its potential role in energy imbalance, learning and memory impairment and Aβ deposition [61]. The present study demonstrated that the expression of phosphorylated mTOR in cortex and hippocampus regions of AD mice were reduced by EA treatment, which may be one reason why EA decreased the accumulation of Aβ in APP/PS1 mice. But this is still not clear whether EA-induced glucose metabolism contributes to eliminate Aβ formation and neurotoxicity. Aβ aggregates can generate reactive oxygen species that cause function impairment of membrane ion-motive ATPases and glucose transporter proteins, which, in turn, disrupts cellular ion homeostasis and energy metabolism [64,65]. Simultaneously, the glucose metabolism impairment in the brain would damage the production of reductive equivalent substances, thus impairing the elimination of free radicals and accelerating Aβ formation in AD [66]. Therefore, the further study is to clarify the relationship among the energy metabolism, free radicals and Aβ formation.

5. Conclusion

The study suggested that AMPK and AKT were activated by EA treatment, further triggered GLUTs to increase the glucose metabolism, and negatively regulated mTOR to induce autophagy and eliminate Aβ deposition (Fig. 16), which delayed the cognitive impairments, particularly in learning and memory ability in AD model mice.

Declaration of interest

The authors declare no financial or commercial conflict of interest.

Acknowledgments

The present study was supported by the National Natural Science Foundation of China (No. 81403450) and the Natural Science Foundation of Fujian Province (No. 2016J01382) and the Foundation of Collaborative Innovation Center of Rehabilitation Technology (Fujian Province) (No. 2016001- collaborative).

Appendix A. Supporting information

Supplementary data associated with this article can be found in the online version at http://dx.doi.org/10.1016/j.freeradbiomed.2017.07.024.

References

[1] D.J. Selkoe, Alzheimer's disease is a synaptic failure, Science 298 (2002) 789–791.
[2] S. Norton, F.E. Matthews, D.E. Barnes, K. Yaffe, C. Brayne, Potential for primary prevention of Alzheimer's disease: an analysis of population-based data, Lancet Neurol. 13 (2014) 788–794.
[3] L.S. Schneider, F. Mangialasche, N. Andreasen, H. Feldman, E. Giacobini, R. Jones, V. Mantua, P. Mecocci, L. Pani, B. Winblad, M. Kivipelto, Clinical trials and late-stage drug development for Alzheimer's disease: an appraisal from 1984 to 2014, J. Intern. Med. 275 (2014) 251–283.
[4] K.Y. Huang, S. Liang, M.L. Yu, S.P. Fu, X. Chen, S.F. Lu, A systematic review and meta-analysis of acupuncture for improving learning and memory ability in

animals, BMC Complement. Altern. Med. 16 (2016) 297.
[5] J.W. Ashford, L. Mahoney, T. Burkett, A role for complementary and integrative medicine in Alzheimer's disease prevention, J. Alzheimers Dis. 48 (2015) 13–14.
[6] R. Lin, J. Chen, X. Li, J. Mao, Y. Wu, P. Zhuo, Y. Zhang, W. Liu, J. Huang, J. Tao, L.D. Chen, Electroacupuncture at the Baihui acupoint alleviates cognitive impairment and exerts neuroprotective effects by modulating the expression and processing of brain-derived neurotrophic factor in APP/PS1 transgenic mice, Mol. Med. Rep. 13 (2016) 1611–1617.
[7] F. Wang, H. Zhong, X. Li, Y. Peng, R. Kinden, W. Liang, X. Li, M. Shi, L. Liu, Q. Wang, L. Xiong, Electroacupuncture attenuates reference memory impairment associated with astrocytic NDRG2 suppression in APP/PS1 transgenic mice, Mol. Neurobiol. 50 (2014) 305–313.
[8] P. Scheltens, K. Blennow, M.M. Breteler, B. de Strooper, G.B. Frisoni, S. Salloway, Flier W.M. Van der, Alzheimer's disease, Lancet 388 (2016) 505–517.
[9] Y. Rui, J.Q. Zheng, Amyloid β oligomers elicit mitochondrial transport defects and fragmentation in a time-dependent and pathway-specific manner, Mol. Brain 9 (2016) 79.
[10] W. Bao, H. Jia, S. Finnema, Z. Cai, R.E. Carson, Y.H. Huang, PET imaging for early detection of Alzheimer's disease: from pathologic to physiologic biomarkers, PET Clin. 12 (2017) 329–350.
[11] C. Duran-Aniotz, C. Hetz, Glucose metabolism: a sweet relief of Alzheimer's disease, Curr. Biol. 26 (2016) R806–R809.
[12] B. Dubois, H.H. Feldman, C. Jacova, S.T. Dekosky, P. Barberger-Gateau, J. Cummings, A. Delacourte, D. Galasko, S. Gauthier, G. Jicha, K. Meguro, J. O'brien, F. Pasquier, P. Robert, M. Rossor, S. Salloway, Y. Stern, P.J. Visser, P. Scheltens, Research criteria for the diagnosis of Alzheimer's disease: revising the NINCDS-ADRDA criteria, Lancet Neurol. 6 (2007) 734–746.
[13] H.F. Wang, L. Tan, L. Cao, X.C. Zhu, T. Jiang, M.S. Tan, Y. Liu, C. Wang, R.M. Tsai, J.P. Jia, J.T. Yu, Alzheimer's disease neuroimaging initiative. Application of the IWG-2 diagnostic criteria for Alzheimer's disease to the ADNI, J. Alzheimers Dis. 51 (2016) 227–236.
[14] S.L. Gardener, H.R. Sohrabi, K.K. Shen, S.R. Rainey-Smith, M. Weinborn, K.A. Bates, T. Shah, J.K. Foster, N. Lenzo, O. Salvado, C. Laske, S.M. Laws, K. Taddei, G. Verdile, R.N. Martins, Cerebral glucose metabolism is associated with verbal but not visual memory performance in community-dwelling older adults, J. Alzheimers Dis. 52 (2016) 661–672.
[15] R. Laforce Jr, D. Tosun, P. Ghosh, M. Lehmann, C.M. Madison, M.W. Weiner, B.L. Miller, W.J. Jagust, G.D. Rabinovici, Parallel ICA of FDG-PET and PiB-PET in three conditions with underlying Alzheimer's pathology, NeuroImage Clin. 4 (2014) 508–516.
[16] A.M. Waldron, C. Wintmolders, A. Bottelbergs, J.B. Kelley, M.E. Schmidt, S. Stroobants, X. Langlois, S. Staelens, In vivo molecular neuroimaging of glucose utilization and its association with fibrillar amyloid-β load in aged APPPS1-21 mice, Alzheimers Res. Ther. 7 (2015) 76.
[17] Y. Lu, J. Ren, S. Cui, J. Chen, Y. Huang, C. Tang, B. Shan, B. Nie, L. Xinsheng, Cerebral glucose metabolism assessment in rat models of Alzheimer's disease: an 18F-FDG-PET study, Am. J. Alzheimers Dis. Other Demen. 31 (2016) 333–340.
[18] D. Wang, X. Li, K. Gao, D. Lu, X. Zhang, C.L. Ma, F. Ye, L. Zhang, Cardiotrophin-1 (CTF1) ameliorates glucose-uptake defects and improves memory and learning deficits in a transgenic mouse model of Alzheimer's disease, Pharmacol. Biochem. Behav. 107 (2013) 48–57.
[19] R.J. Mark, Z. Pang, J.W. Geddes, K. Uchida, M.P. Mattson, Amyloid beta-peptide impairs glucose transport in hippocampal and cortical neurons: involvement of membrane lipid peroxidation, J. Neurosci. 17 (1997) 1046–1054.
[20] D. Kapogiannis, M.P. Mattson, Disrupted energy metabolism and neuronal circuit dysfunction in cognitive impairment and Alzheimer's disease, Lancet Neurol. 10 (2011) 187–198.
[21] J.A. Godoy, J.A. Rios, J.M. Zolezzi, N. Braidy, N.C. Inestrosa, Signaling pathway cross talk in Alzheimer's disease, Cell Commun. Signal. 12 (2014) 23.
[22] A. Rickle, N. Bogdanovic, I. Volkman, B. Winblad, R. Ravid, R.F. Cowburn, Akt activity in Alzheimer's disease and other neurodegenerative disorders, Neuroreport 15 (2004) 955–959.
[23] da-Silva-G.S. Seixas, H.M. Melo, M.V. Lourenco, N.M. Lyra, E-Silva, M.B. de-Carvalho, S.V. Alves-Leon, J.M. de Souza, W.L. Klein, W.S. da-Silva, S.T. Ferreira, F.G. De-Felice, Amyloid-β oligomers transiently inhibit AMP-activated kinase and cause metabolic defects in hippocampal neurons, J. Biol. Chem. 292 (2017) 7395–7406.
[24] R.M. Uranga, N.P. Alza, M.A. Conde, S.S. Antollini, G.A. Salvador, Phosphoinositides: two-path signaling in neuronal response to oligomeric amyloid β peptide, Mol. Neurobiol. 54 (2017) 3236–3252.
[25] S. Kang, N.R. Moon, da S. Kim, S.H. Kim, S. Park, Central acylated ghrelin improves memory function and hippocampal AMPK activation and partly reverses the impairment of energy and glucose metabolism in rats infused with β-amyloid, Peptides 71 (2015) 84–93.
[26] D. Zhou, W. Zhou, J.K. Song, Z.Y. Feng, R.Y. Yang, S. Wu, L. Wang, A.L. Liu, G.H. Du, DL0410, a novel dual cholinesterase inhibitor, protects mouse brains against Aβ-induced neuronal damage via the Akt/JNK signaling pathway, Acta Pharmacol. Sin. 37 (2016) 1401–1412.
[27] W. Dong, W. Guo, X. Zheng, F. Wang, Y. Chen, W. Zhang, H. Shi, Electroacupuncture improves cognitive deficits associated with AMPK activation in SAMP8 mice, Metab. Brain Dis. 30 (2015) 777–784.
[28] A. Tominaga, N. Ishizaki, Y. Naruse, H. Kitakoji, Y. Yamamura, Repeated application of low-frequency electroacupuncture improves high-fructose diet-induced insulin resistance in rats, Acupunct. Med. 29 (2011) 276–283.
[29] S. Rojas, J.R. Herance, J.D. Gispert, S. Abad, E. Torrent, X. Jiménez, D. Pareto, U. Perpiña, S. Sarroca, E. Rodríguez, A. Ortega-Aznar, C. Sanfeliu, In vivo evaluation of amyloid deposition and brain glucose metabolism of 5XFAD mice using positron emission tomography, Neurobiol. Aging 34 (2013) 1790–1798.
[30] Y.F. Zhang, J.C. Yu, X.Z. Zhang, J.X. Han, Effect of acupuncture intervention on hippocampal neuron loss and astrocytosis in SAMP 8 mice, Zhen Ci Yan Jiu 38 (2013) 358–364.
[31] R.A. Bevins, J. Besheer, Object recognition in rats and mice: a one-trial non-matching-to-sample learning task to study 'recognition memory', Nat. Protoc. 1 (2006) 1306–1311.
[32] J.Q. Tong, J. Zhang, M. Hao, J. Yang, Y.F. Han, X.J. Liu, H. Shi, M.N. Wu, Q.S. Liu, J.S. Qi, Leptin attenuates the detrimental effects of β-amyloid on spatial memory and hippocampal later-phase long term potentiation in rats, Horm. Behav. 73 (2015) 125–130.
[33] C. Li, M. Xie, F. Luo, C. He, J. Wang, G. Tan, Z. Hu, The extremely low-frequency magnetic field exposure differently affects the AMPAR and NMDAR subunit expressions in the hippocampus, entorhinal cortex and prefrontal cortex without effects on the rat spatial learning and memory, Environ. Res. 134 (2014) 74–80.
[34] P.J. Pistell, M. Zhu, D.K. Ingram, Acquisition of conditioned taste aversion is impaired in the amyloid precursor protein/presenilin 1 mouse model of Alzheimer's disease, Neuroscience 152 (2008) 594–600.
[35] S.A. Ferguson, S. Sarkar, L.C. Schmued, Longitudinal behavioral changes in the APP/PS1 transgenic Alzheimer's disease model, Behav. Brain Res. 242 (2013) 125–134.
[36] D.S. Roy, A. Arons, T.I. Mitchell, M. Pignatelli, T.J. Ryan, S. Tonegawa, Memory retrieval by activating engram cells in mouse models of early Alzheimer's disease, Nature 531 (2016) 508–512.
[37] B.J. Culliton, NIH says "yes" to acupuncture, Nat. Med. 3 (1997) 1307.
[38] Z.L. Sun, J. Liu, W. Guo, T. Jiang, C. Ma, W.B. Li, Y.L. Tang, S.H. Ling, Serum brain-derived neurotrophic factor levels associate with cognitive improvement in patients with schizophrenia treated with electroacupuncture, Psychiatry Res. 244 (2016) 370–375.
[39] T. Guo, Z. Guo, W. Zhang, W. Ma, X. Yang, X. Yang, J. Hwang, X. He, X. Chen, T. Ya, Electroacupuncture and cognitive behavioural therapy for sub-syndromal depression among undergraduates: a controlled clinical trial, Acupunct. Med. 34 (2016) 356–363.
[40] W.G. Dong, F. Wang, Y. Chen, X.H. Zheng, Y.C. Xie, W.Q. Guo, H. Shi, Electroacupuncture reduces Aβ production and BACE1 expression in SAMP8 Mice, Front. Aging Neurosci. 7 (2015) 148.
[41] X. Li, F. Guo, Q. Zhang, T. Huo, L. Liu, H. Wei, L. Xiong, Q. Wang, Electroacupuncture decreases cognitive impairment and promotes neurogenesis in the APP/PS1 transgenic mice, BMC Complement. Altern. Med. 14 (2014) 37.
[42] C.A. Castellano, S. Nugent, N. Paquet, S. Tremblay, C. Bocti, G. Lacombe, H. Imbeault, É. Turcotte, T. Fulop, S.C. Cunnane, Lower brain 18F-fluorodeoxyglucose uptake but normal 11C-acetoacetate metabolism in mild Alzheimer's disease dementia, J. Alzheimers Dis. 43 (2015) 1343–1353.
[43] L. Mosconi, J. Murray, M. Davies, S. Williams, E. Pirraglia, N. Spector, W.H. Tsui, Y. Li, T. Butler, R.S. Osorio, L. Glodzik, S. Vallabhajosula, P. McHugh, C.R. Marmar, M.J. de Leon, Nutrient intake and brain biomarkers of Alzheimer's disease in at-risk cognitively normal individuals: a cross-sectional neuroimaging pilot study, BMJ Open 4 (2014) e004850.
[44] S. Rapic, H. Backes, T. Viel, M.P. Kummer, P. Monfared, B. Neumaier, S. Vollmar, M. Hoehn, Linden A. Van der, M.T. Heneka, A.H. Jacobs, Imaging microglial activation and glucose consumption in a mouse model of Alzheimer's disease, Neurobiol. Aging 34 (2013) 351–354.
[45] C. Kuntner, A.L. Kesner, M. Bauer, R. Kremslehner, T. Wanek, M. Mandler, R. Karch, J. Stanek, T. Wolf, M. Müller, O. Langer, Limitations of small animal PET imaging with [18F]FDDNP and FDG for quantitative studies in a transgenic mouse model of Alzheimer's disease, Mol. Imaging Biol. 11 (2009) 236–240.
[46] Y. Huang, C. Tang, S. Wang, Y. Lu, W. Shen, J. Yang, J. Chen, R. Lin, S. Cui, H. Xiao, S. Qu, X. Lai, B. Shan, Acupuncture regulates the glucose metabolism in cerebral functional regions in chronic stage ischemic stroke patients–a PET-CT cerebral functional imaging study, BMC Neurosci. 13 (2012) 75.
[47] J. Yang, F. Zeng, Y. Feng, L. Fang, W. Qin, X. Liu, W. Song, H. Xie, J. Chen, F. Liang, A PET-CT study on the specificity of acupoints through acupuncture treatment in migraine patients, BMC Complement. Altern. Med. 12 (2012) 123.
[48] Y. Huang, J. Chen, W.M. Htut, X. Lai, G. Wik, Acupuncture increases cerebral glucose metabolism in human vascular dementia, Int. J. Neurosci. 117 (2007) 1029–1037.
[49] J. Jiang, K. Gao, Y. Zhou, A. Xu, S. Shi, G. Liu, Z. Li, Electroacupuncture treatment improves learning-memory ability and brain glucose metabolism in a mouse model of Alzheimer's disease: using Morris water maze and micro-PET, Evid. Based Complement. Altern. Med. 2015 (2015) 142129.
[50] X. Lai, J. Ren, Y. Lu, S. Cui, J. Chen, Y. Huang, C. Tang, B. Shan, B. Nie, Effects of acupuncture at HT7 on glucose metabolism in a rat model of Alzheimer's disease: an 18F-FDG-PET study, Acupunct. Med. 34 (2016) 215–222.
[51] Y. Lu, Y. Huang, C. Tang, B. Shan, S. Cui, J. Yang, J. Chen, R. Lin, H. Xiao, S. Qu, X. Lai, Brain areas involved in the acupuncture treatment of AD model rats: a PET study, BMC Complement. Altern. Med. 14 (2014) 178.
[52] S.J. Vannucci, F. Maher, I.A. Simpson, Glucose transporter proteins in brain: delivery of glucose to neurons and glia, Glia 21 (1997) 2–21.
[53] G.R. Steinberg, B.E. Kemp, AMPK in health and disease, Physiol. Rev. 89 (2009) 1025–1078.
[54] P. Vijayaraj, C. Kröger, U. Reuter, R. Windoffer, R.E. Leube, T.M. Magin, J. Cell Biol. 187 (2009) 175–184.
[55] S.R. Kimball, Interaction between the AMP-activated protein kinase and mTOR signaling pathways, Med. Sci. Sports Exerc. 38 (2008) 1958–1964.
[56] C.C. Dibble, L.C. Cantley, Regulation of mTORC1 by PI3K signaling, Trends Cell

Biol. 25 (2015) 545–555.
[57] A. Salminen, K. Kaarniranta, A. Haapasalo, H. Soininen, M. Hiltunen, AMP-activated protein kinase: a potential player in Alzheimer's disease, J. Neurochem. 118 (2011) 460–474.
[58] K.A. DiTacchio, S.F. Heinemann, G. Dziewczapolski, Metformin treatment alters memory function in a mouse model of Alzheimer's disease, J. Alzheimers Dis. 44 (2015) 43–48.
[59] S. Kang, N.R. Moon, da S. Kim, S.H. Kim, S. Park, Central acylated ghrelin improves memory function and hippocampal AMPK activation and partly reverses the impairment of energy and glucose metabolism in rats infused with β-amyloid, Peptides 71 (2015) 84–93.
[60] R. Zheng, Z.H. Zhang, C. Chen, Y. Chen, S.Z. Jia, Q. Liu, J.Z. Ni, G.L. Song, Selenomethionine promoted hippocampal neurogenesis via the PI3K-Akt-GSK3β-Wnt pathway in a mouse model of Alzheimer's disease, Biochem. Biophys. Res. Commun. 485 (2017) 6–15.
[61] H. Liu, H. Qiu, Q. Xiao, W. Le, Chronic hypoxia-induced autophagy aggravates the neuropathology of Alzheimer's disease through AMPK-mTOR signaling in the APPSwe/PS1dE9 mouse model, J. Alzheimers Dis. 48 (2015) 1019–1032.
[62] V. Vingtdeux, L. Giliberto, H. Zhao, P. Chandakkar, Q. Wu, J.E. Simon, E.M. Janle, J. Lobo, M.G. Ferruzzi, P. Davies, P. Marambaud, AMP-activated protein kinase signaling activation by resveratrol modulates amyloid-beta peptide metabolism, J. Biol. Chem. 285 (2010) 9100–9113.
[63] Q. Li, Y. Liu, M. Sun, Autophagy and Alzheimer's disease, Cell. Mol. Neurobiol. 37 (2017) 377–388.
[64] C. Dias, C.F. Lourenço, E. Ferreiro, R.M. Barbosa, J. Laranjinha, A. Ledo, Age-dependent changes in the glutamate-nitric oxide pathway in the hippocampus of the triple transgenic model of Alzheimer's disease: implications for neurometabolic regulation, Neurobiol. Aging 46 (2016) 84–95.
[65] N. Abolhassani, J. Leon, Z. Sheng, S. Oka, H. Hamasaki, T. Iwaki, Y. Nakabeppu, Molecular pathophysiology of impaired glucose metabolism, mitochondrial dysfunction, and oxidative DNA damage in Alzheimer's disease brain, Mech. Ageing Dev. 161 (Pt A) (2017) 95–104.
[66] C.R. Williams, J.L. Gooch, Calcineurin Aβ regulates NADPH oxidase (Nox) expression and activity via nuclear factor of activated T cells (NFAT) in response to high glucose, J. Biol. Chem. 289 (2014) 4896–4905.